SYNTHESIS AND CHARACTERIZATION OF SEVERAL PYRIDINE IONIC LIQUIDS AND THEIR COMPLEX SALTS WITH SOME TRANSITION ELEMENTS, THERMAL STABILITY, AND THERMODYNAMIC INVESTIGATION

Israa A. Saeed[1], Assim A. Sabah[2*]

[1]Department of Chemistry, College of Science, University of Mosul, Iraq
[2]Department of Science, College of Basic Education, University of Mosul, Iraq

Received 13.04.2026
Accepted 08.06.2026

***Abstract**: 4-ethylpyridine was reacted with allyl bromide and then with allyl iodide to create two ionic liquids from substituted pyridine [AEtPy]Br (E1) and [AEtPy]I (E2). Characterization methods, including mass spectrometry, elemental analysis, and ^{1}H and ^{13}C NMR spectroscopy, were employed to characterize the newly developed ionic liquids. Following preparation, complex salts were produced by reacting the ionic liquids with Lewis acids ($MnCl_2$, $FeCl_2$, $CoCl_2$, $NiCl_2$, $CuCl_2$, and $ZnCl_2$) at a 2:1 molar ratio of ionic liquid to metal chloride. The tetrahedral structure of these complex salts was confirmed using spectroscopic and physical methods, including magnetic susceptibility, atomic absorption spectroscopy, and UV-Vis spectroscopy. The primary objective of the study was to investigate the thermal properties of ionic liquids using thermogravimetric analysis (TGA) to determine their thermodynamic parameters. Thermal data were collected using a MODEL-FITTING APPROACH and the authorized mathematical formulas. Results confirmed the compounds' stability and potential for future use.*
***Keywords:** pyridinium ionic liquids, complex salts, thermal analysis*

1. Introduction

Considering their wide range of applications and ease of production, ionic liquids have gained increasing importance in recent years [1, 2]. These properties highlight their significance, as does the well-established ability to tailor their characteristics by modifying either or both the cations and anions [3, 4]. In addition to their aforementioned chemical and physical properties, ionic liquids have attracted the interest of biochemists, environmental scientists, and medical professionals due to their strong biological activity. Their biological activity has become increasingly important in medicine and pharmaceuticals because of their toxicity against a variety of bacteria and fungi, offering potential applications in the pharmaceutical sector. Ionic liquids are promising materials for many contemporary applications, including battery electrolytes, active pharmaceutical ingredients, biocatalysts, catalysts for chemical reactions, and biopolymer processing [5].

Pyridine forms several ionic liquids due to the presence of a nitrogen atom, which enhances their stability. The properties of ionic liquids depend on the length of the hydrocarbon chain, the type of alkyl group substituted on the nitrogen atom, and the type of anion. Consequently, like other ionic liquids, pyridine-based ionic liquids can contain different substituent groups [6, 7]. Conventional and environmentally friendly solvent-free methods have been used to prepare substituted pyridinium bromides (benzyl/4-nitrobenzyl-substituted quaternary ammonium pyridinium bromide). The nontoxic nature and straightforward reaction setup of the solvent-free solid-phase (greener) approach make it superior to the traditional method. Pharmacokinetics plays a crucial role in validating a target and transforming a lead compound into a medication [8].

Pyridine-based ionic liquids have been utilized in a range of applications. N-butylpyridinium tetrachloroferrate ($[C_4py]FeCl_4$), a magnetically separable catalyst, was created to extract trace olefins from aromatic hydrocarbons. A simple synthetic method was employed to prepare the magnetic ionic liquid, which was then thoroughly characterized by FTIR, TGA/DTG, DTA, UV-visible, and Raman spectroscopy. The effects of various reaction parameters, including molar ratio, temperature, time, and ionic liquid reusability, were then examined. The ionic liquid ($[C_4py]FeCl_4$), containing 5% catalyst by weight, at 70 °C for 12 minutes, demonstrated superior olefin removal

performance. An external magnet facilitated the simple extraction of the magnetic IL from the solution, enabling effective recovery without purification or work-up procedures [9, 10].

Another application involves the hydrolytic activity of lipase, which was not significantly affected by the addition of ionic liquids to an aqueous solvent but was more pronounced in methanol. The hydrolytic activity of lipase may be enhanced by the addition of [C6Py]Br ionic liquid as a methanol co-solvent (10:5 methanol:ionic liquid). When pyridinium ionic liquids are used as a co-solvent in a methanol system, the hydrolytic activity of lipase can be increased by approximately 15.61%. Molecular dynamics analysis of the interaction between lipase and ionic liquids validated the experimental findings. The lipase conformation was more stable in the ionic liquid containing bromide as the anion, which generally results in short-range interactions between the lipase and bromide anion [11, 12].

Pyridine ionic liquids with various anions have numerous additional applications. Therefore, research into the thermal stability of ionic liquids is crucial, particularly for their industrial applications. If the sample is not fully decomposed, which can take an extended period, depending on the temperature range, accurate kinetic analysis of thermal decomposition may be limited. As a result, both isothermal and non-isothermal experiments help provide a thorough understanding of the kinetic and thermodynamic behavior of thermal decomposition reactions [13, 14].

Environmental contamination from industrial effluents, especially sulfur compounds in fuel streams and heavy metal ions in wastewater, is becoming a more significant worldwide concern. Therefore, there is an urgent need for sophisticated and sustainable separation materials [15, 16]. Because of their exceptional thermal and chemical stability, strong coordination affinity for metal ions and sulfur-containing species, and structural tunability, ionic liquids and their complex salts offer a promising platform for the logical design of task-specific and recyclable systems [17]. To create new complex salts, this study synthesized novel pyridine-based ionic liquids with a complex chemical structure and then reacted them with specific transition-metal Lewis acids. To assess the stability of the prepared compounds and to support future use in environmental remediation procedures, a thorough investigation of their thermal behavior and thermodynamic parameters was conducted.

2. Experimental part

2.1. Preparation of pyridinium ionic liquids: *1-allyl-4-ethylpyridinium bromide* [AEtPy]Br (**E1**) and *1-allyl-4-ethylpyridinium iodide* [AEtPy]I (**E2**)

All chemicals used were pure and high-quality (Sigma-Aldrich, Fluka, Alpha, and DBH). Following the literature [17-19], ionic liquids were synthesized by reacting para-ethylpyridine, a pyridine substitute, with allyl bromide and allyl iodide. To guarantee an uninterrupted reaction, a minimal excess of allyl halide was added to the pyridine substitute, one mole at a time. After stirring for half an hour, the reaction was refluxed for 2 hours. Following the reaction, the unreacted allyl halide was removed from the resultant product by washing it with hexane, yielding a pure pyridinium halide ionic liquid.

2.2. *Preparation and Characterizations of Complex Salts [AEtPy]$_2$[MCl$_2$X$_2$] (1-12).* As illustrated in Scheme 1, the ionic liquid was reacted with metal chloride in a 1:2 ratio to produce the complex salts of the ionic liquid. To prepare the ionic liquid, 4-ethylpyridine and an allyl halide were combined in a 1:1 molar ratio and stirred continuously for 2 hours. This reaction is endothermic. To increase the product's yield, more allyl halide was added. Upon completion, the product was formed, and the unreacted allyl halide was removed by repeatedly washing it with hexane. By reacting molar ratios (2:1) of the [AEtPy]X: metal chloride, some transition metal complexes were created. The metal chloride dissolved in water (10 mL) was added gradually to the ionic liquid dissolved in a suitable volume of ethanol (10 mL). The mixture was then stirred continuously for two hours. The complex salt precipitates after the reaction is finished, the solution is filtered, and the precipitate is cleaned with diethyl ether. The solution is then concentrated to half its volume by evaporation and left overnight.

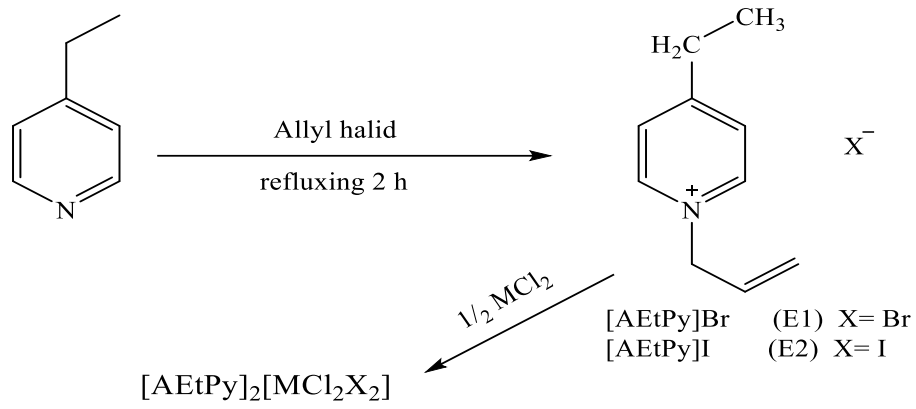

M = Mn, X = Br (1) M = Mn, X = I (7)
M = Fe, X = Br (2) M = Fe, X = I (8)
M = Ni, X = Br (3) M = Ni, X = I (9)
M = Co, X = Br (4) M = Co, X = I (10)
M = Cu, X = Br (5) M = Cu, X = I (11)
M = Zn, X = Br (6) M = Zn, X = I (12)

Scheme 1. Preparation of ionic liquids and complex salts.

In addition to other measurements, such as electrical conductivity and melting point, the compounds were characterized using physical and spectroscopic techniques. DMSO-d_6 was used as a solvent for ^{1}H-NMR (Bruker Avance DPX, 400 MHz) and energy-dispersive X-ray Spectroscopy (EDX) on a TESCAN MIRA3 (Czechia). A Trio-1000 mass spectrometer was used for GC-MS (Supporting documents: Figure S1 and S2); Shimadzu performed an infrared spectrum (Supporting documents: Figure S3). Simultaneously, the SensAA GCB scientific equipment system (Avanta 2.02 software) measured the atomic absorption. The electronic spectrum was measured using a Shimadzu 1800 UV-Vis spectrometer; the melting point was measured using an Electrothermal Melting Point 9100; and the magnetic susceptibility was measured using a Sherwood MK1. METTLER TOLEDO TGA-DSC with STARe evaluation software (V 19.00) was used to perform the thermal study. The HANNA EC214 conductivity meter was used to measure conductivity.

2.3. *Thermal Study.* A Mettler Toledo thermal study was carried out using STAR^e software version 19, with the following program (temperature 35-600°C) and a ceramic pan with a temperature rise of 10°C per minute under standard air cooling and water cooling in the heating furnace used. A heating rate of 10°C/min is reasonable for observing the substance's decomposition. The thermal diagrams of complex salts are shown in the supporting documents (Figures S4 and S5). The "MODEL-FITTING APPROACH" method was used to determine thermodynamic values by first calculating the activation energy from the thermal decomposition curve and then determining the enthalpy, entropy, and free energy changes.

2.4. *Thermodynamic Parameters.* The first-order reaction rate equation, given in Equations (1) and (2), was used to compute the rate constant and reaction half-life using TGA data, including DTG, activation energy, and other thermodynamic parameters, accounting for all phase transformations as first-order reactions [20, 21].

$$\frac{dy}{dx} = k\,(1 - X) \qquad (1)$$

$$X = \frac{Wi - Wt}{Wi - Wf} \qquad (2)$$

W_i represents the sample's initial weight, W_t its weight at time t, and W_f its final weight. Equation (1) can be rewritten as follows:

$$ln\,(1\text{-}X) = -Kt \qquad (3)$$

The data for each phase showed a straight line when plotted using equation (3), confirming that the transformations were first-order reactions. The half-life (t1/2) was determined using equation (4), and the rate constant (k) value for each phase was obtained from the slope of each line.

$$t1/2 \ = \frac{0.693}{K} \qquad (4)$$

The Standard Test Approach: The kinetic study is carried out using the **nth** order kinetics model, the standard test method for decomposition kinetics by thermogravimetric analysis. The kinetic energy is determined using equations (5) and (6); for the first iteration, b equals 0.457 K^{-1} and the slope is (k), which is equivalent to $\Delta(\log)/(1/\beta)\Delta T$. Equation (6), where T is the temperature at constant conversion for the heating rate nearest to the midpoint of the experimental heating rates, E is also the activation energy ($J{\cdot}mol^{-1}$), A is the pre-exponential factor, and β is the heating rate, is also the value of an integral approximation for the refined value of $E(RT)^{-1}$ [22, 23].

$$Ea = -\left(\frac{R}{b}\right) \times [log\beta / \left(\frac{1}{T}\right)] \qquad (5)$$

$$K = A\, e^{-(Ea/RT)} \qquad (6)$$

3. Results and discussion

Physical and spectroscopic techniques were used to identify the compounds. A few characteristic results for the prepared compounds are provided in Table 1.

Table 1. Some physical data of prepared compounds.

No.	Comp.	m.p °C	Colour	Cond.*	M%**
E1	[AEtPy]Br	< 25	Brown	90	---
E2	[AEtPy]I	< 25	Brown	90	---
1	$[AEtPy]_2[MnCl_2Br_2]$	100>	Brown	130	9.67
2	$[AEtPy]_2[FeCl_2Br_2]$	100>	Black	135	9.45
3	$[AEtPy]_2[CoCl_2Br_2]$	100>	Blue	145	11.45
4	$[AEtPy]_2[NiCl_2Br_2]$	100>	Blue	162	10.88
5	$[AEtPy]_2[CuCl_2Br_2]$	100>	Olive	142	9.56
6	$[AEtPy]_2[ZnCl_2Br_2]$	100>	Brown	152	13.00
7	$[AEtPy]_2[MnCl_2I_2]$	100>	Brown	163	9.32
8	$[AEtPy]_2[FeCl_2I_2]$	100>	Black	147	8.25
9	$[AEtPy]_2[CoCl_2I_2]$	100>	Blue	135	8.67
10	$[AEtPy]_2[NiCl_2I_2]$	100>	Black	156	8.63
11	$[AEtPy]_2[CuCl_2I_2]$	100>	Green	145	9.28
12	$[AEtPy]_2[ZnCl_2I_2]$	100>	Brown	145	9.52
* Conductivity: $ohm^{-1}.\ cm^2.\ mol^{-1}$ by using DMSO as solvent at 25°C.					
** Metal % found in the compound					

Observing that the mass spectral results and the elemental analysis results of the prepared ionic liquids closely match the literature on the identification of these compounds [13, 24, 25]. Furthermore, Figures 1-4 display these compounds' nuclear magnetic resonance (NMR) spectra and mass fragmentation:

[AEtPy]Br (E1) characteristics data: ^{1}H-NMR (500 MHz, DMSO) δ 8.95 (d, 2H), 8.05 (d, J = 6.3 Hz, 2H), 6.20 – 6.08 (m, 1H), 5.44 – 5.34 (m, 2H), 5.24 (d, J = 6.2 Hz, 2H), 2.91 (q, J = 7.6 Hz, 2H), 1.24 (t, J = 7.5 Hz, 3H). ^{13}C-NMR (126 MHz, DMSO) δ 164.13, 144.01, 131.78, 127.29, 121.60, 61.46, 40.02, 39.85, 39.69, 39.52, 39.35, 39.19, 39.02, 27.97, 13.37. CHN data

(Cal./Found): C, 52.65/50.93; H, 6.19/6.08; Br, 35.03/37.12; N, 6.14/5.85. Spectral data: 10121, 17513, 21505, 28169 cm^{-1}.

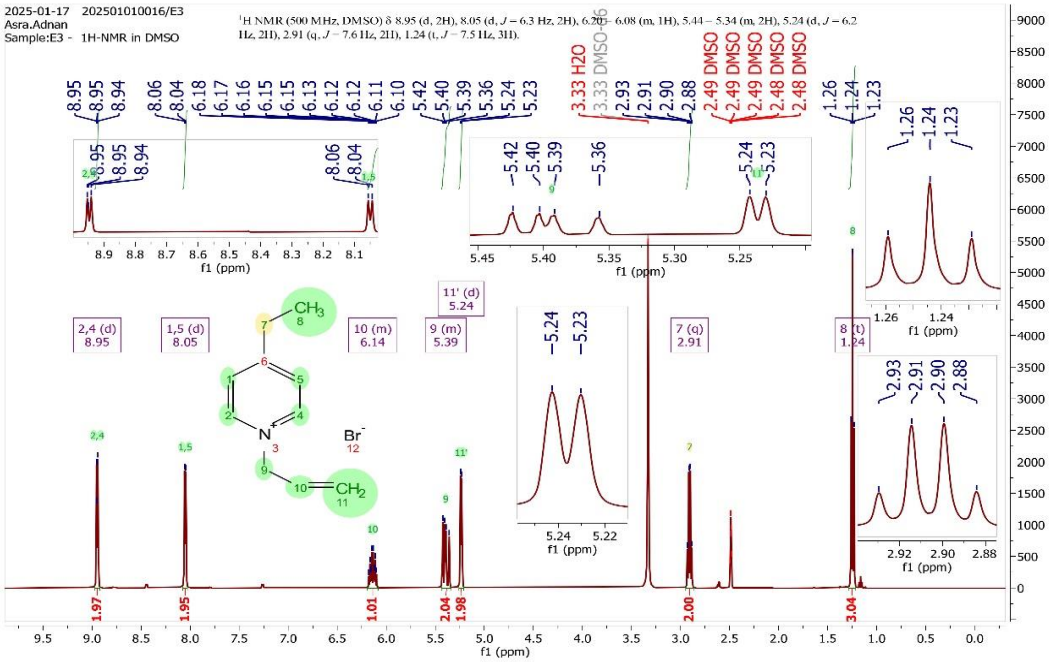

Fig. 1. The H^1-NMR spectrum of [AEtPy]Br (E1)

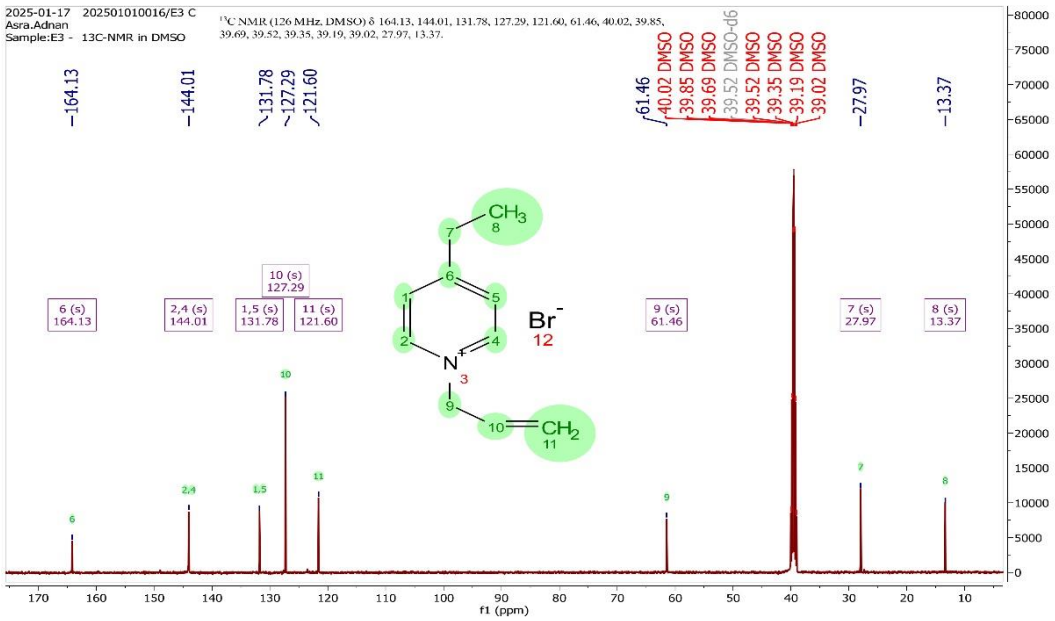

Fig. 2. The C^{13}-NMR spectrum of [AEtPy]Br (E1)

[AEtPy]I (E2) characteristics data: ^{1}H NMR (500 MHz, DMSO) δ 8.95(d, *J* = 6.9 Hz, 2H), 8.07(d, *J* = 6.9 Hz, 2H), 6.21 – 6.09 (m, 1H), 5.44 – 5.36 (m, 2H), 5.27 (d, *J* = 6.3 Hz, 2H), 2.91 (q, *J* = 7.5 Hz, 2H), 1.23 (t, *J* = 7.5 Hz, 3H). ^{13}C NMR (126 MHz, DMSO) δ 164.05, 143.80, 131.54, 127.27, 121.75, 61.34, 27.94, 13.37. CHN data (Cal./Found): C, 43.66/43.22; H, 5.13/5.02; I, 46.12/47.22; N,5.09/5.21. Spectral data:22075,37175cm^{-1}.

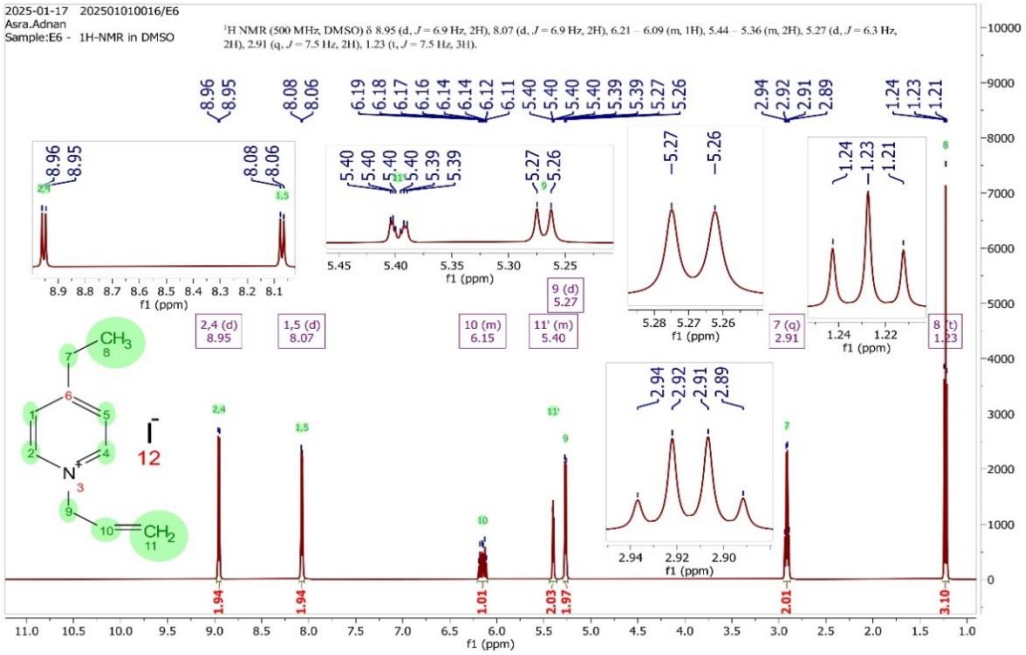

Fig. 3. The H^1-NMR spectrum of [AEtPy]I (E2)

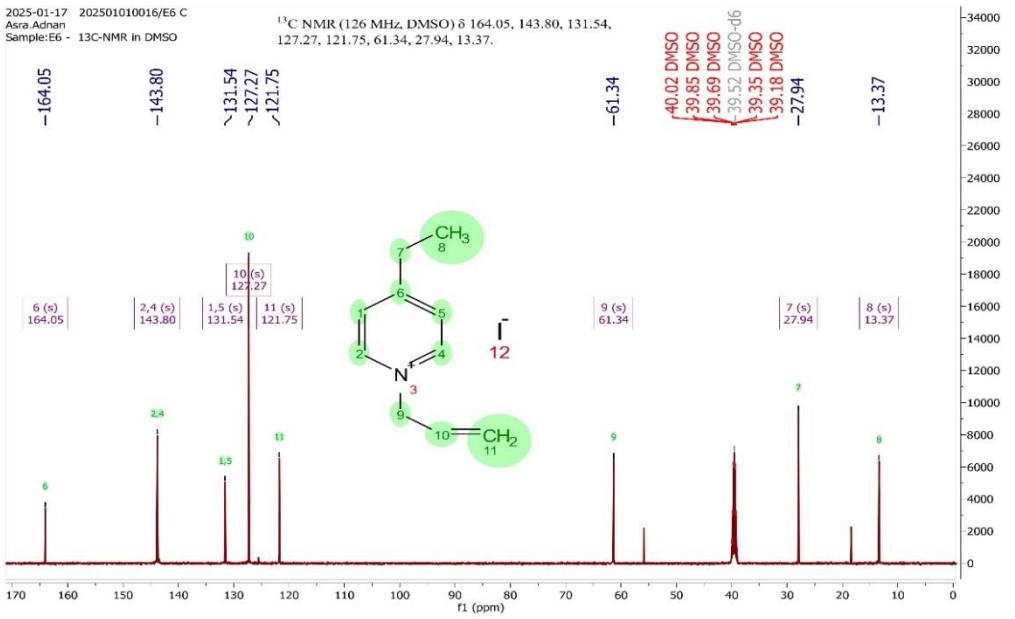

Fig. 4. The C^{13}-NMR spectra of [AEtPy]I (E2)

Physical characteristics and spectral data were also used to characterize the transition-metal complex salts produced [26, 27]. Spectral and magnetic susceptibility data confirmed the tetrahedral structure of the complex salts surrounding the metal ion. The ratio created by binding one mole of ionic liquid to one mole of Lewis acid (metal chloride) was validated by the experimental metal content. Transition elements exhibit different magnetic properties depending on their oxidation state and spatial configuration, which, in turn, depends on the number of lone electrons. Several factors, including the nature of the ligand, the size of the metal, and the oxidation state, influence this number. These differences are clearly evident between manganese (II), which has five lone electrons and gives a magnetic moment value of 5.8 B.M., and zinc (II), which exhibits a zero value as a diamagnetic complex due to the absence of lone electrons in its proposed tetrahedral configuration.

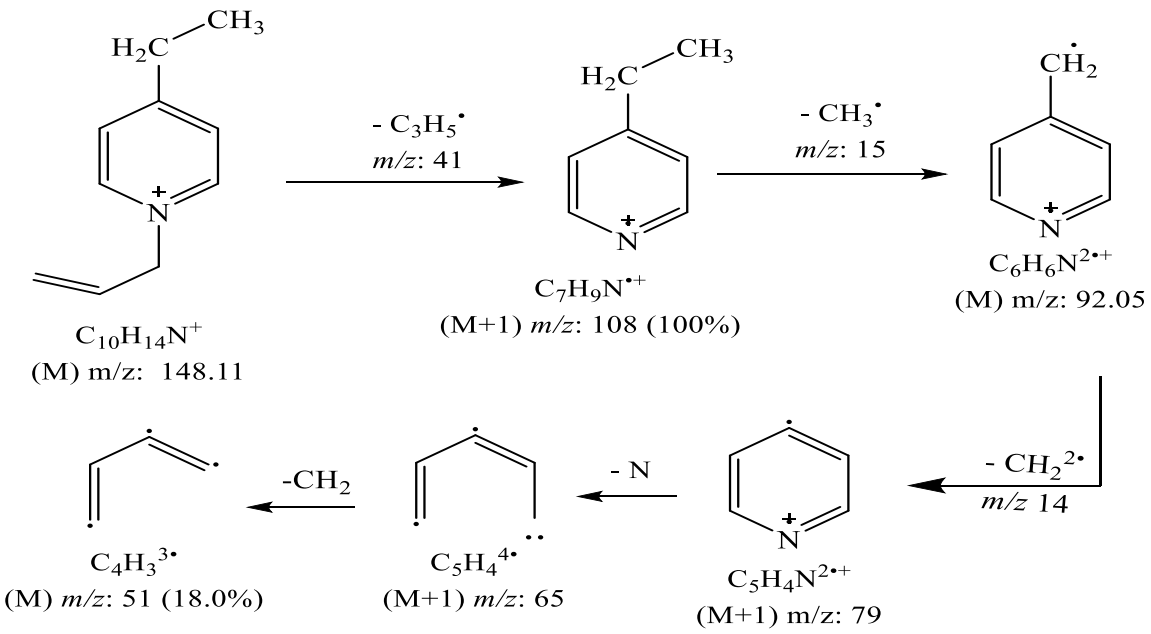

Scheme 2. Suggested fragmentation of cation mass spectroscopy of E1 and E2

The ferrous complexes also exhibit high magnetic susceptibility values, similar to the anion complex, showing an effective magnetic moment of 5.72 B.M. and absorption bands at (11961, 12562 cm^{-1}), which are very close to those of the ferrous salt complexes prepared in this study. Similarly, the cobalt (II), nickel (II), and copper (II) complexes show effective magnetic moments of 4.2, 3.61, and 2.42 B.M., respectively, and absorption bands at 14836, 16477, 17761, 12610, 14164, and 14310 cm^{-1}. These data are largely consistent with those from this study, confirming the proposed tetrahedral shape around the central metal ion in the anion of the complex salt [25]. Some information about the prepared complex salts is shown in Table 2.

Table 2. Some spectral and magnetic data of prepared compounds.

Comp. No.	**Bands** cm^{-1}	**Transitions**	μ_{eff}(B.M)	**geometry**
1	37175	$^6A_1 \rightarrow {}^4T_1$ G.T	5.8	tetrahedral
2	37736	$^5E \rightarrow {}^5T_2$ G.T	4.5	tetrahedral
3	14970,16502	$^4A_2 \rightarrow {}^4T_2$ $^4A_2 \rightarrow {}^4T_1$ $^4A_2 \rightarrow {}^4T_1$ G.T	3.8	tetrahedral
4	10163,11351	$^3T_1 \rightarrow {}^3T_2$ $^3T_1 \rightarrow {}^3A_2$ $^3T_1 \rightarrow {}_3T_1$	3.1	tetrahedral
5	10941,11274,33333	$^2T_2 \rightarrow {}^2E$ G.T	2.2	tetrahedral
6	10267,11351,37453	$^6A_1 \rightarrow {}^4T_1$ G.T	---	tetrahedral
7	10152,11351,23923, 29851, 39216	$^6A_1 \rightarrow {}^4T_1$ G.T	5.9	tetrahedral
8	10152, 11351, 27548	$^5E \rightarrow {}^5T_2$ G.T	4.7	tetrahedral
9	14925, 16502, 19493	$^4A_2 \rightarrow {}^4T_2$ $^4A_2 \rightarrow {}^4T_1$ $^4A_2 \rightarrow {}^4T_1$	4.1	tetrahedral

		G.T		
10	10152, 11351, 28329, 38610	$^3T_1 \rightarrow {}^3T_2$ $^3T_1 \rightarrow {}^3A_2$ $^3T_1 \rightarrow {}_3T_1$	2.2	tetrahedral
11	39063	$^2T_2 \rightarrow {}^2E$ G.T	1.8	tetrahedral
12	10163, 11325, 23923, 38610	$^6A_1 \rightarrow {}^4T_1$ G.T	---	tetrahedral

The distinctive (C=C) stretching vibration of the pyridine aromatic ring was detected in the 1612–1639 cm^{-1} region when the stretching frequencies of the prepared ionic liquids E1 and E2 and their corresponding complex salts were analyzed. In the ranges of 1423–1498 cm^{-1} and 1153–1205 cm^{-1}, respectively, the principal stretching bands that corresponded to (C=N) and (C–N) vibrations were visible. Furthermore, the 3034–3076 cm^{-1} region showed the (C–H) stretching vibrations. In the 2930–2980 cm^{-1} range, a new distinctive band was discovered that was ascribed to the (N^+–allyl) functional group. Every absorption band observed has good match values previously published in the literature, confirming the suggested structure [17, 25, 28]. The spectra and magnetic sensitivity indicate that the expected structure around the metal ion is tetrahedral, consistent with extensive previous research. All these results are consistent with the scientific values for the tetrahedral structure around the atom or central ion [17, 18].

3.1. Thermal Behavior. Examining the thermal stability and thermodynamic properties of the produced compounds, particularly the ionic liquids, is a primary goal of this study. Determining the thermal stability of these compounds and comparing them to one another and to previously prepared pyridine ionic liquids are the primary objectives of this investigation and data collection [13, 29].
The effects of anion displacement on the thermal properties of pyridinium ionic liquids have been investigated and contrasted. The produced ionic liquids have a moisture content of 7-10, as indicated by thermal analysis. Thermal decomposition between 100 and 120 °C can be considered an indication of this. This result is consistent with many ionic liquid preparations. When comparing ionic liquids 1 and 2, there are no appreciable differences between the two substances at this point in their thermal breakdown.

There is only one main stage of decomposition for pure ionic liquids, according to the thermal curves (Fig. 5). In the temperature range of 179 to 350°C, Compound 1 thermally breaks down, dissociating 78% of the tested sample. Compound 2 starts to break down at 166°C and dissociates 75% of its mass at 395°C. The ionic liquid's purity, thermal stability before these temperatures, and suitability for any industrial use or application within its stable temperature range are all indicated by the fact that the decomposition process proceeds through only one central stage.

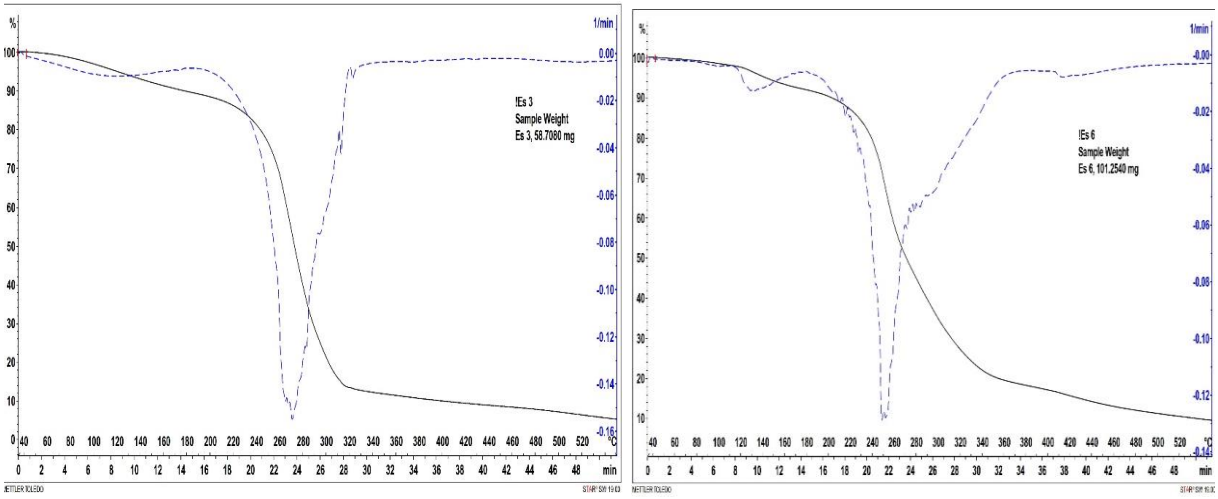

Fig. 5. The TGA and DTG for [AEtPy]Br (E1) and [AEtPy]I (E2)

Compared with other compounds [17, 25, 30], the thermal stability of compounds 1 and 2 is good and can be controlled in the future by adjusting the charge of the negative ion. It can also be adjusted by altering the substituted alkyl group, or both, to achieve the desired thermal properties appropriate for the anticipated scientific applications involving ionic liquids.

Using the MODEL-FITTING APPROACH in the 19th edition of the thermal analysis software to find thermodynamic values was the second step in the thermal study. As illustrated in Fig. 6, this investigation yielded the equilibrium constant for the thermal decomposition kinetics and the activation energy for the thermal decomposition curve [31, 32].

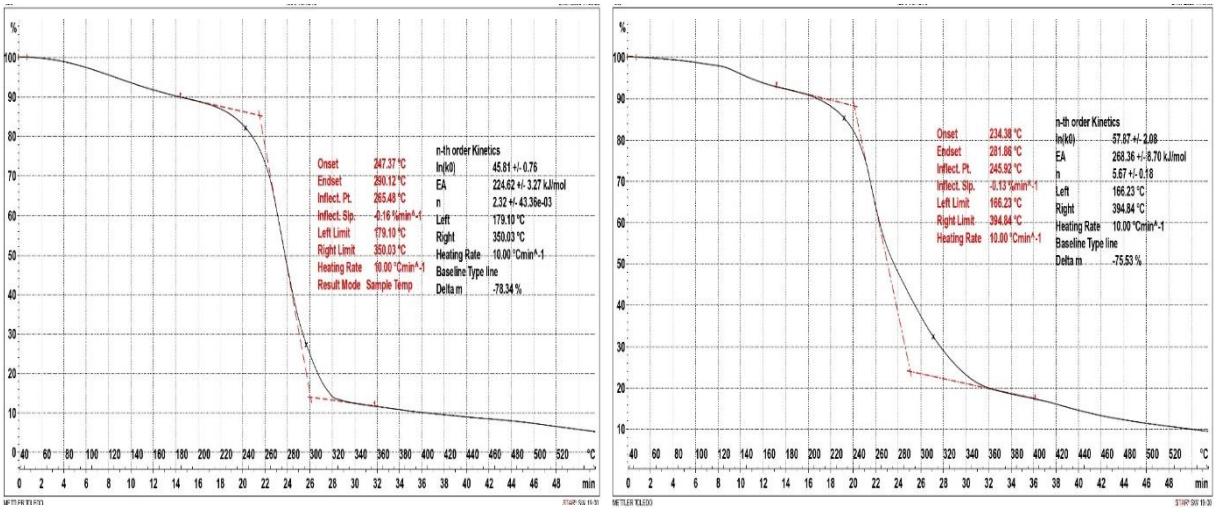

Fig. 6. The MODEL-FITTING APPROACH of the TGA curve of [AEtPy]Br (E1)

The data gathered using the MODEL-FITTING APPROACH method are displayed in Table 3 and include the activation energy, half-life, reaction rate constant, and thermodynamic values for thermal decomposition.

Table 3. Kinetic data and thermodynamic parameters

Comp.	Temp. K^{-1}	k min^{-1}	$t_{1/2}$ min	E_a ($Jmol^{-1}$)	ΔH ($Jmol^{-1}$)	ΔS ($Jmol^{-1}K^{-1}$)	ΔG ($Jmol^{-1}$)
E1	542	0.16	4.33	224620	222383	40163	182220
E2	531	0.13	5.33	268360	266214	61586	204628

Conclusion

The results indicate the presence of metal in the complex salts, which form a tetrahedral structure surrounded by halogens. The thermal analysis also demonstrated that the thermodynamic constants of the ionic liquids are slightly affected by variations in the halide or anion, and that they are thermally stable within a suitable range. In addition to this information, it can be inferred that these prepared ionic liquids can function as solvents or catalysts in a variety of green chemistry-related reactions because of their stability. This has a favorable effect on numerous environmental applications designed to protect the environment from risks, particularly those posed by the buildup of hazardous chemicals, such as heavy fuel desulfurization and heavy metal removal.

Supporting Documents.

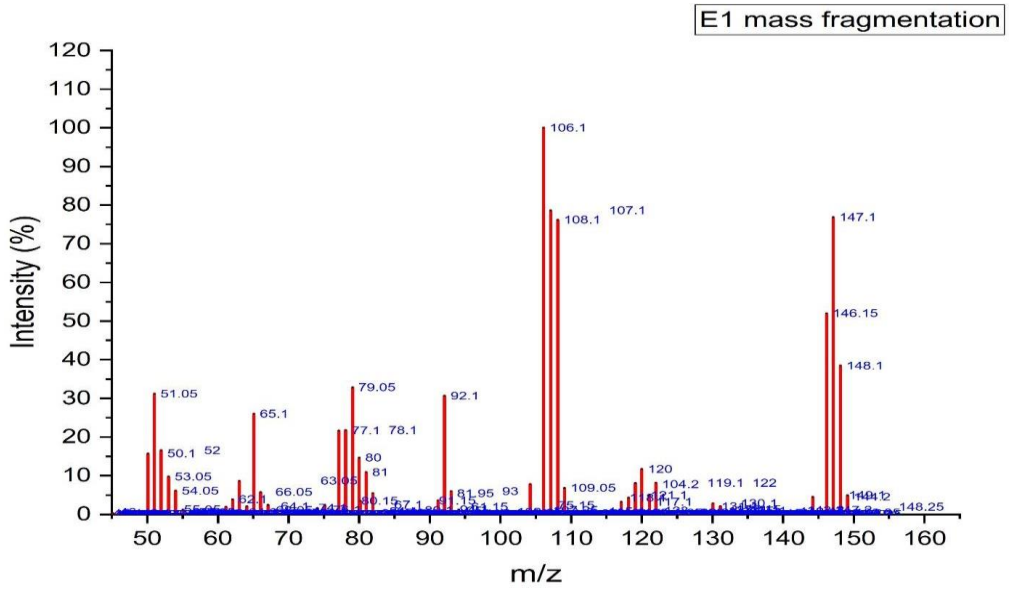

Fig. S1. Mass spectroscopy of [AEtPy]Br (E1)

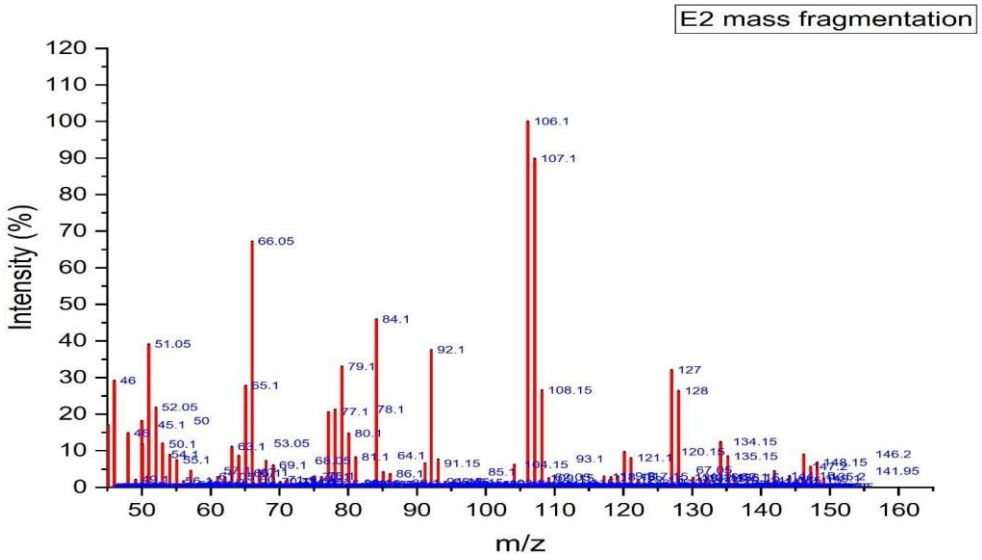

Fig. S2. Mass spectroscopy of [AEtPy]I (E2)

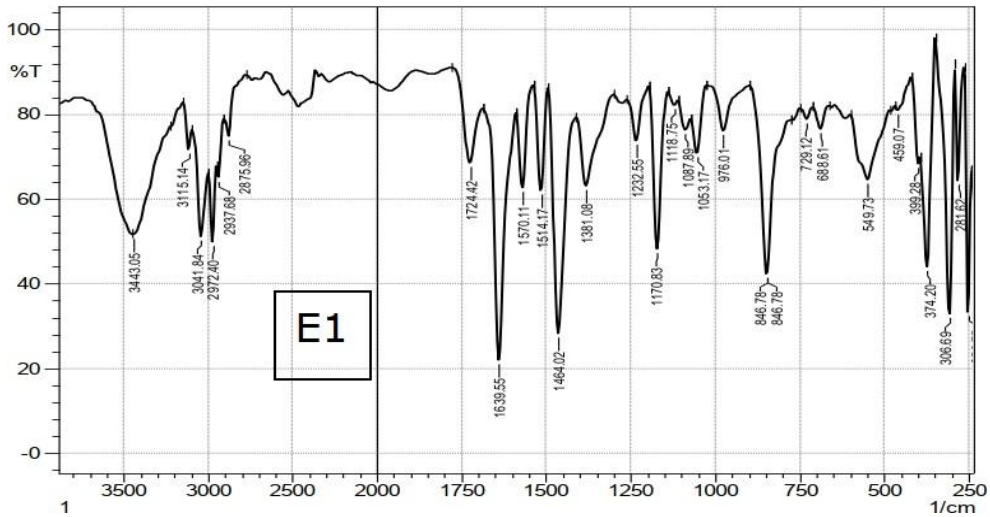

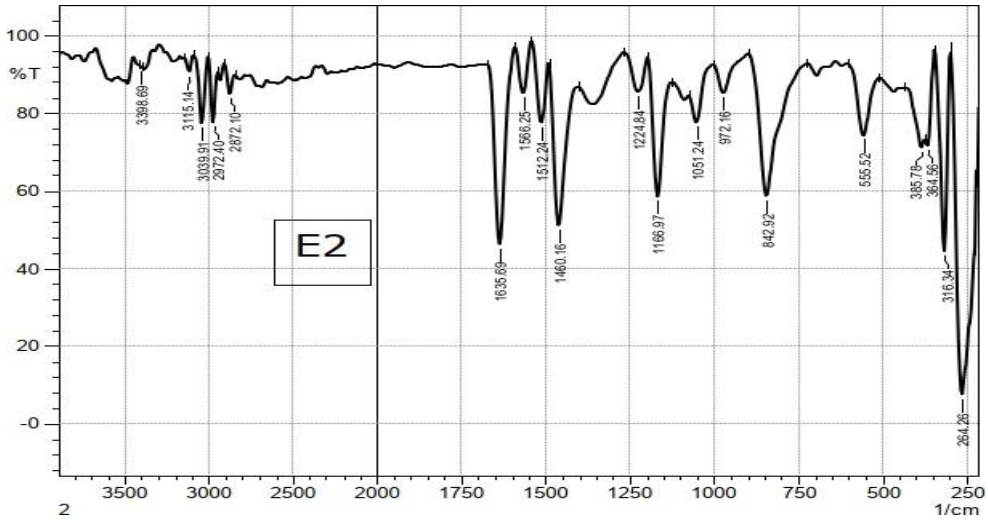
E2
%T
100
80
60
40
20
-0
3388.69
3115.14
3039.91
2972.40
2872.10
1635.69
1566.25
1512.24
1460.16
1224.84
1166.97
1051.24
972.16
842.92
555.52
385.78
364.56
316.34
264.26
3500
3000
2500
2000
1750
1500
1250
1000
750
500
250
1/cm
2

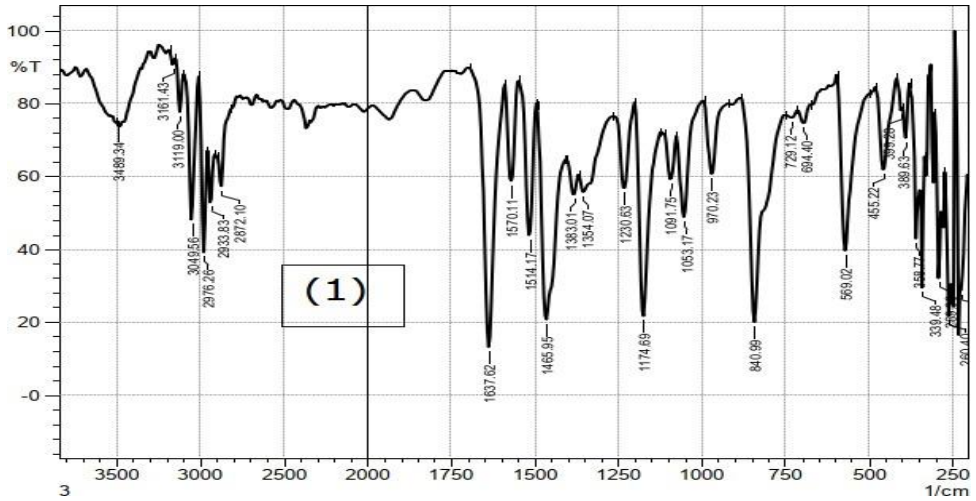
(1)
%T
100
80
60
40
20
-0
3488.34
3161.43
3119.00
3049.56
2976.26
2933.83
2872.10
1637.02
1570.11
1514.17
1466.95
1383.01
1354.07
1260.65
1174.69
1091.75
1053.17
970.23
840.99
729.12
694.40
569.02
455.22
388.63
339.48
3500
3000
2500
2000
1750
1500
1250
1000
750
500
250
1/cm
3

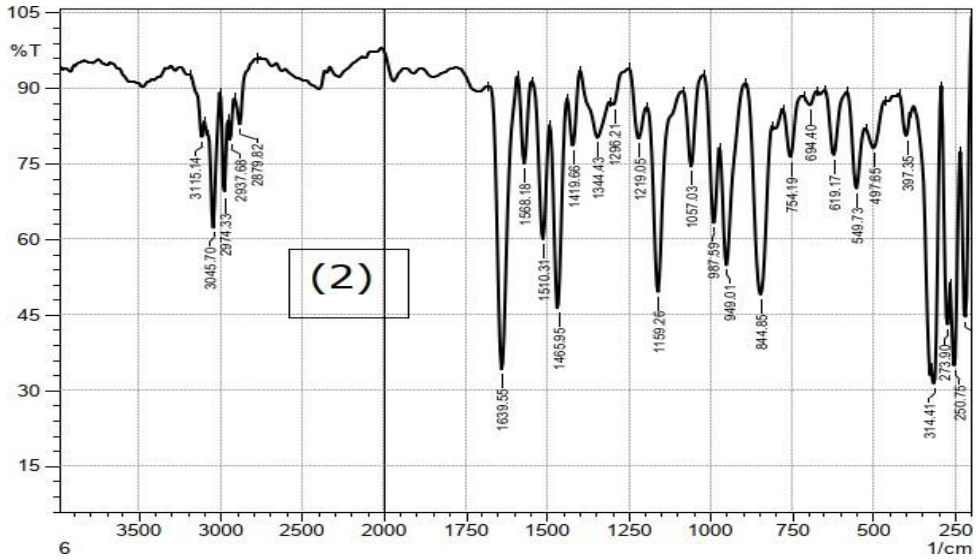
(2)
%T
105
90
75
60
45
30
15
3115.14
3045.70
2974.33
2937.68
2879.82
1639.55
1568.18
1510.31
1465.95
1419.66
1344.43
1296.21
1219.05
1159.26
1057.03
987.59
949.01
844.85
754.19
694.40
619.17
549.73
497.68
397.35
314.41
273.90
250.75
3500
3000
2500
2000
1750
1500
1250
1000
750
500
250
1/cm
6

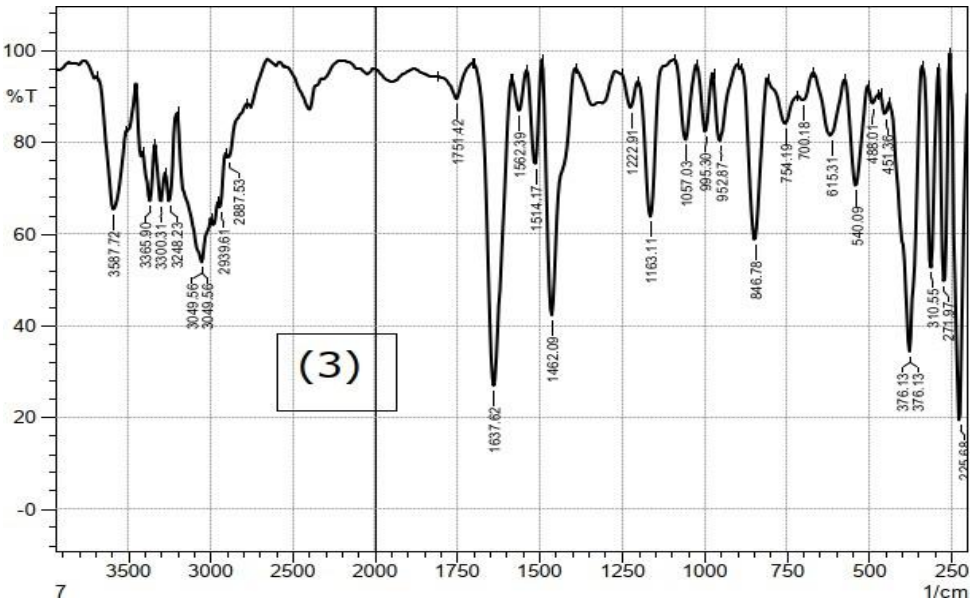
100
%T
80
60
40
20
-0
3587.72
3365.90
3300.31
3248.23
3049.56
3039.56
2939.61
2887.53
1751.42
1637.62
1562.39
1514.17
1462.09
1222.91
1163.11
1057.03
995.30
952.87
846.78
754.19
700.18
615.31
540.09
488.01
451.36
376.13
376.13
310.55
271.97
(3)
7
3500
3000
2500
2000
1750
1500
1250
1000
750
500
250
1/cm

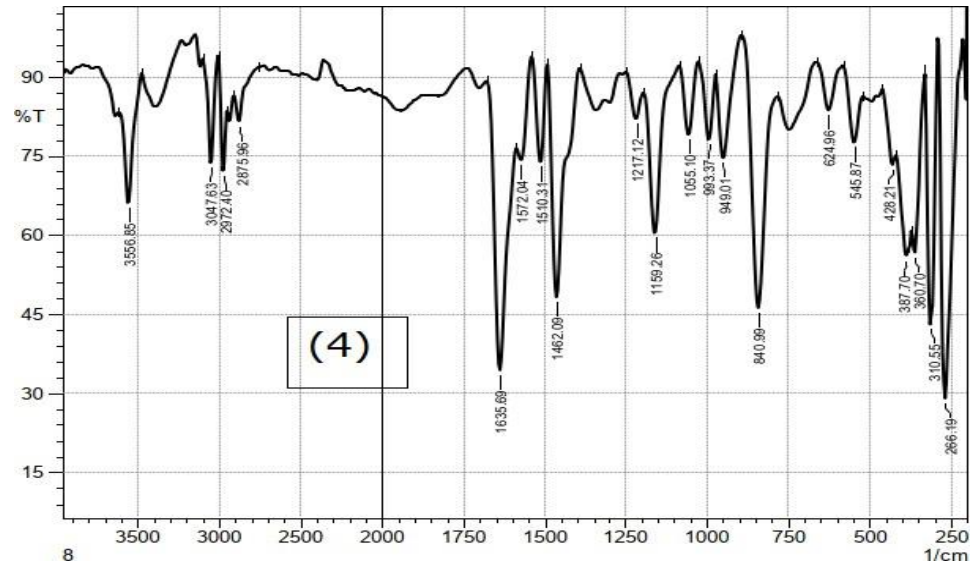
90
%T
75
60
45
30
15
3556.85
3047.63
2972.40
2875.96
1635.69
1572.04
1510.31
1462.09
1217.12
1159.26
1055.10
993.37
949.01
840.99
624.96
545.87
428.21
387.70
360.70
310.55
266.19
(4)
8
3500
3000
2500
2000
1750
1500
1250
1000
750
500
250
1/cm

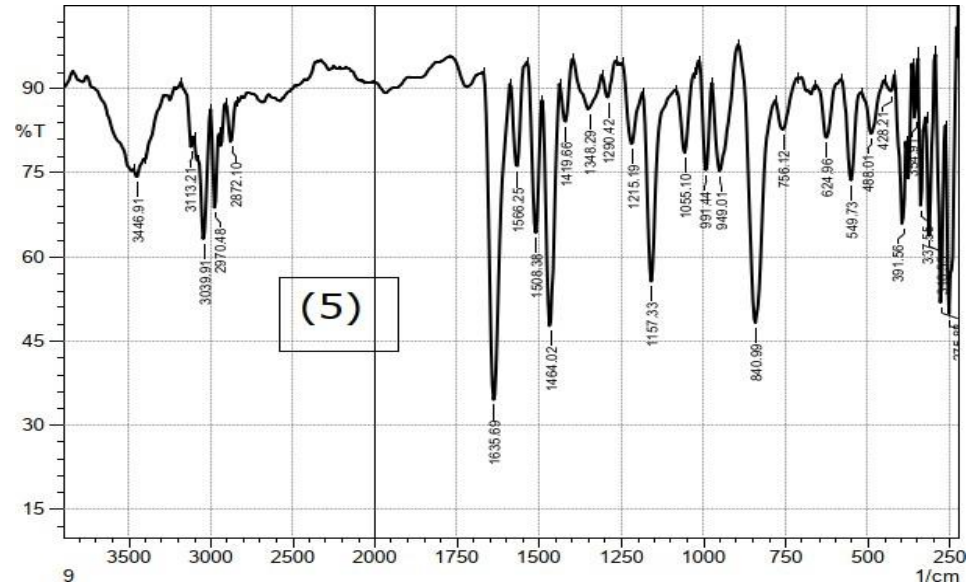
90
%T
75
60
45
30
15
3446.91
3113.21
3039.91
2970.48
2872.10
1635.69
1566.25
1508.38
1464.02
1419.66
1348.29
1290.42
1215.19
1157.33
1055.10
991.44
949.01
840.99
756.12
624.96
549.73
488.01
428.21
391.56
(5)
9
3500
3000
2500
2000
1750
1500
1250
1000
750
500
250
1/cm

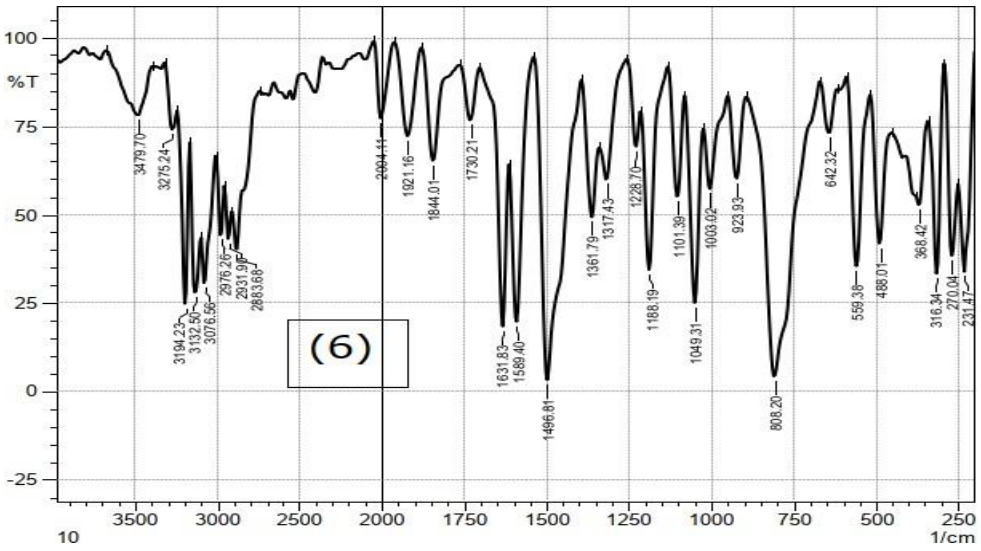
%T
100
75
50
25
0
-25
3479.70
3275.24
3194.23
3132.50
3076.56
2976.26
2931.98
2883.68
2004.41
1921.16
1844.01
1730.21
1631.83
1589.40
1496.81
1361.79
1317.43
1228.70
1188.19
1101.39
1049.31
1003.02
923.93
808.20
642.32
558.38
488.01
368.42
316.34
270.04
231.47
(6)
10
3500
3000
2500
2000
1750
1500
1250
1000
750
500
250
1/cm

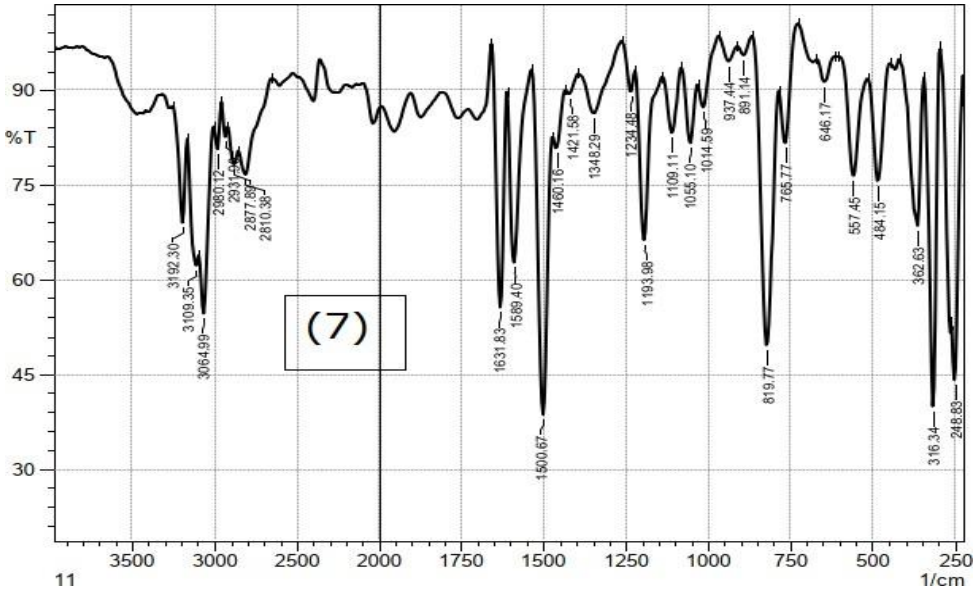
%T
90
75
60
45
30
3192.30
3109.35
3064.99
2980.12
2937.78
2877.80
2810.38
1631.83
1589.40
1500.67
1460.16
1421.58
1348.29
1234.48
1193.98
1109.11
1055.10
1014.58
937.44
891.14
819.77
765.77
646.17
557.45
484.15
362.63
316.34
248.83
(7)
11
3500
3000
2500
2000
1750
1500
1250
1000
750
500
250
1/cm

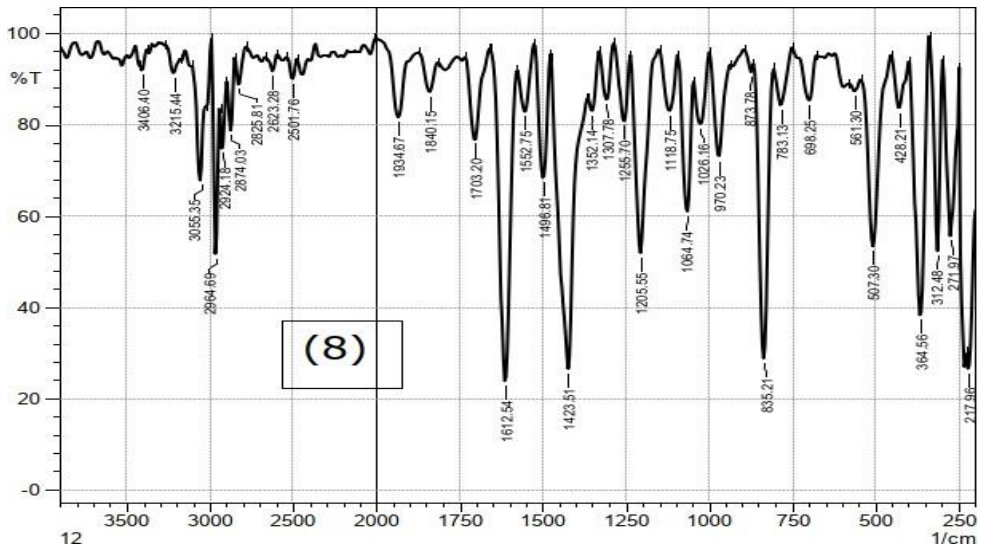
%T
100
80
60
40
20
-0
3406.40
3215.44
3055.35
2964.69
2924.18
2874.03
2825.81
2623.28
2501.76
1934.67
1840.15
1703.20
1612.54
1552.75
1496.81
1425.51
1352.14
1307.78
1255.70
1205.55
1118.75
1064.74
1026.16
970.23
873.78
835.21
783.13
698.25
561.30
507.30
428.21
364.56
312.48
271.97
217.96
(8)
12
3500
3000
2500
2000
1750
1500
1250
1000
750
500
250
1/cm

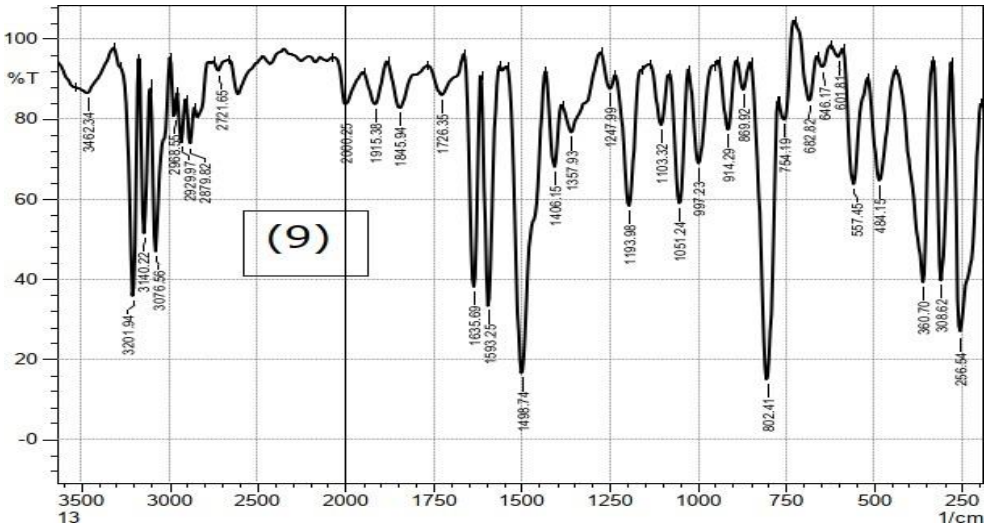
100
%T
80
60
40
20
-0
3462.34
3201.94
3140.22
3076.56
2968.55
2929.97
2879.82
2721.65
2000.25
1915.38
1845.94
1726.35
1635.69
1593.25
1498.74
1406.15
1357.93
1247.99
1193.98
1103.32
1051.24
997.23
914.29
869.92
754.19
682.82
646.17
601.81
557.45
494.15
360.70
308.62
266.54
802.41
(9)
3500
3000
2500
2000
1750
1500
1250
1000
750
500
250
13
1/cm

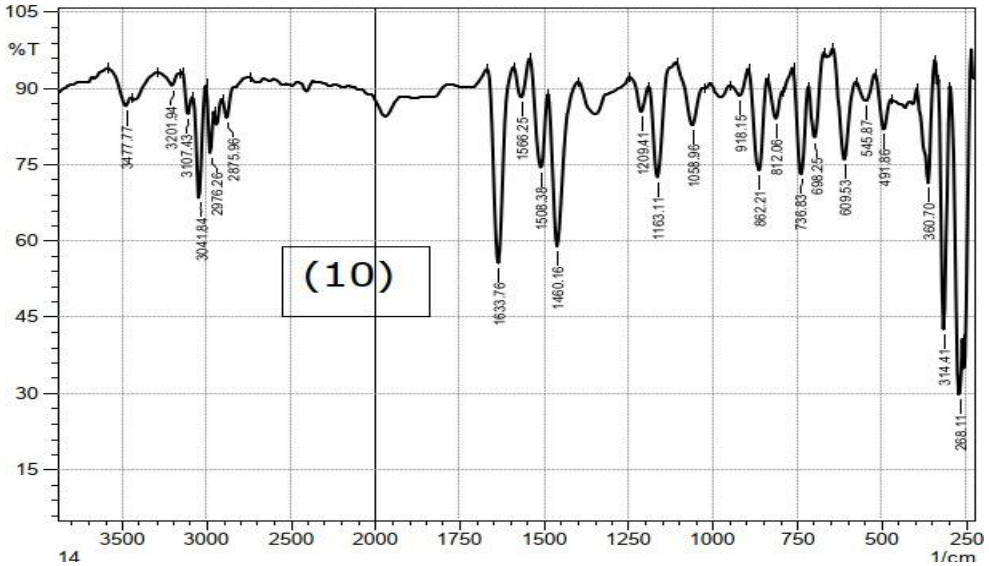
105
%T
90
75
60
45
30
15
3477.77
3201.94
3107.43
3041.84
2976.26
2875.96
1633.76
1566.25
1508.38
1460.16
1209.41
1163.11
1058.96
918.15
862.21
812.06
736.83
698.25
609.53
545.87
491.86
360.70
314.41
268.11
(10)
3500
3000
2500
2000
1750
1500
1250
1000
750
500
250
14
1/cm

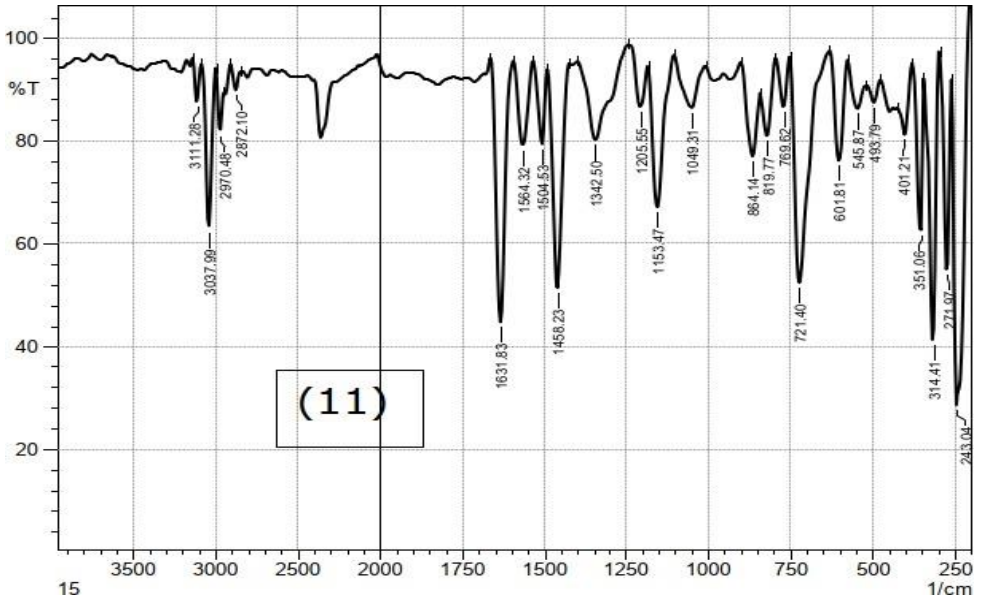
100
%T
80
60
40
20
3111.28
2970.48
2872.10
3037.99
1631.83
1564.32
1504.53
1458.23
1342.50
1205.55
1153.47
1049.31
864.14
819.77
769.62
721.40
601.81
545.87
493.79
401.21
351.06
314.41
271.97
243.04
(11)
3500
3000
2500
2000
1750
1500
1250
1000
750
500
250
15
1/cm

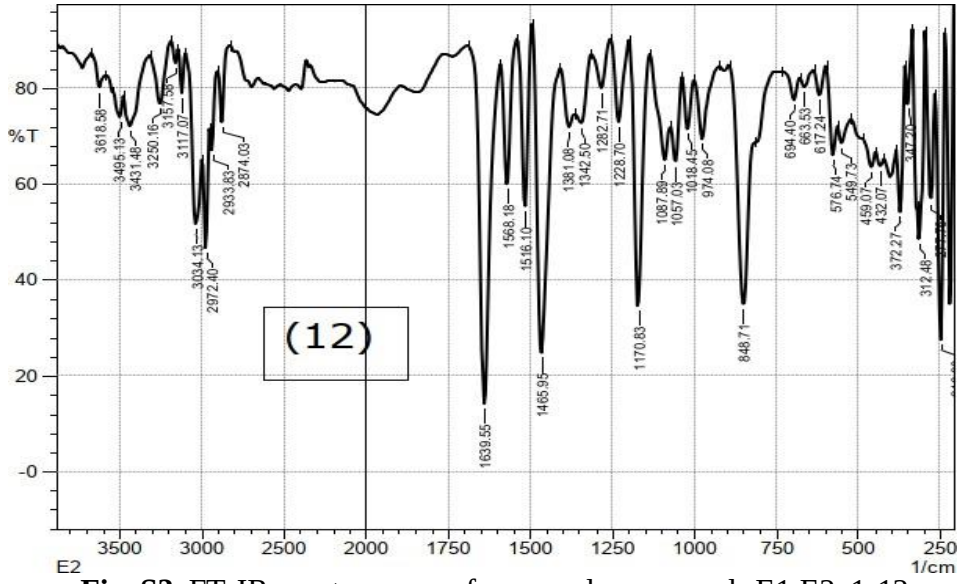

Fig. S3. FT-IR spectroscopy of prepared compounds E1,E2, 1-12

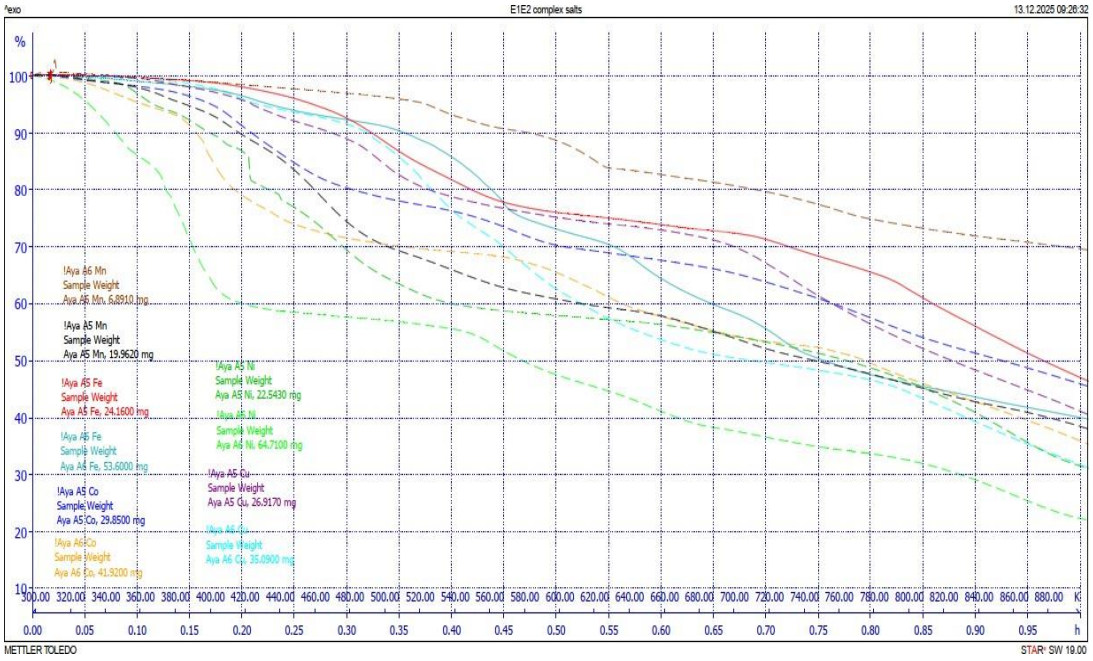

Fig. S4. The TGA curves of most prepared complex salts

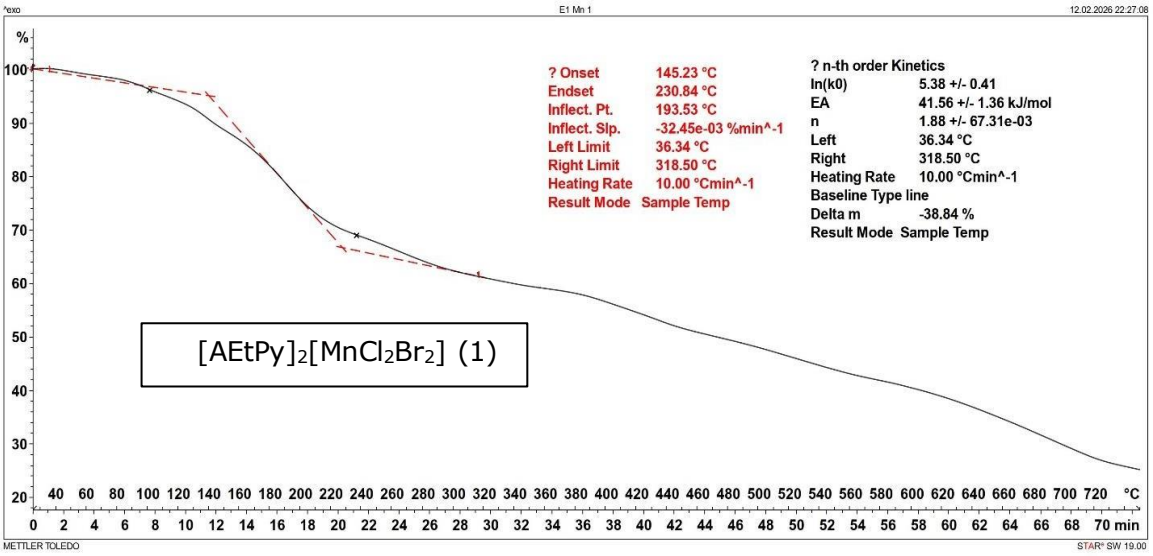
^exo
E1 Mn 1
12.02.2026 22:27:08
%
? Onset 145.23 °C
Endset 230.84 °C
Inflect. Pt. 193.53 °C
Inflect. Slp. -32.45e-03 %min^-1
Left Limit 36.34 °C
Right Limit 318.50 °C
Heating Rate 10.00 °Cmin^-1
Result Mode Sample Temp
? n-th order Kinetics
ln(k0) 5.38 +/- 0.41
EA 41.56 +/- 1.36 kJ/mol
n 1.88 +/- 67.31e-03
Left 36.34 °C
Right 318.50 °C
Heating Rate 10.00 °Cmin^-1
Baseline Type line
Delta m -38.84 %
Result Mode Sample Temp
[AEtPy]2[MnCl2Br2] (1)
°C
70 min
METTLER TOLEDO
STAR° SW 19.00

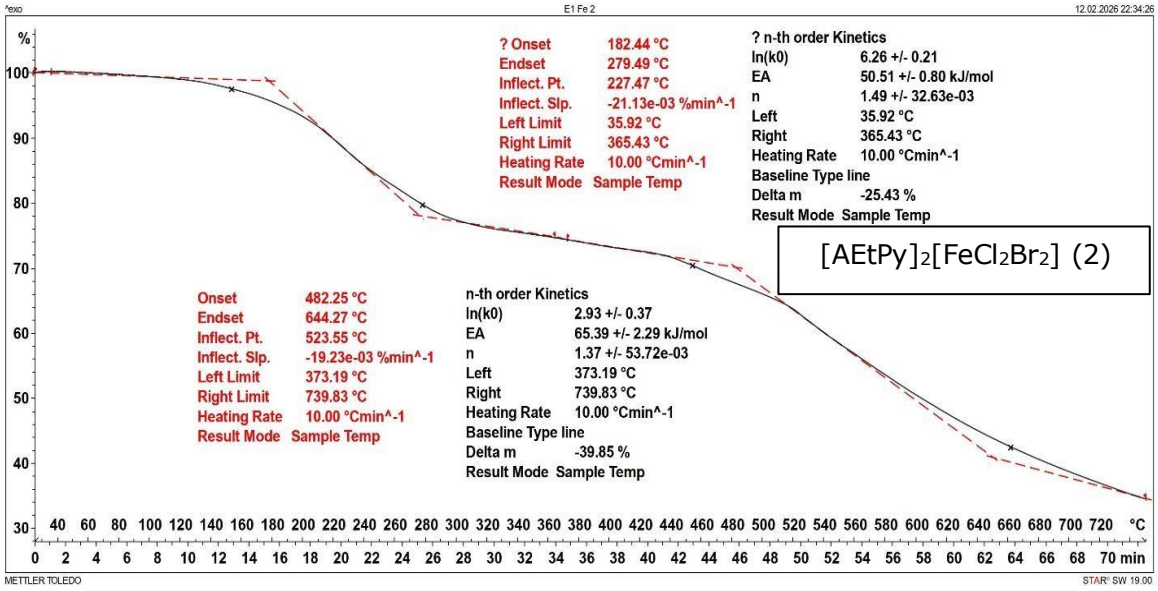
^exo
E1 Fe 2
12.02.2026 22:34:26
%
? Onset 182.44 °C
Endset 279.49 °C
Inflect. Pt. 227.47 °C
Inflect. Slp. -21.13e-03 %min^-1
Left Limit 35.92 °C
Right Limit 365.43 °C
Heating Rate 10.00 °Cmin^-1
Result Mode Sample Temp
? n-th order Kinetics
ln(k0) 6.26 +/- 0.21
EA 50.51 +/- 0.80 kJ/mol
n 1.49 +/- 32.63e-03
Left 35.92 °C
Right 365.43 °C
Heating Rate 10.00 °Cmin^-1
Baseline Type line
Delta m -25.43 %
Result Mode Sample Temp
[AEtPy]2[FeCl2Br2] (2)
Onset 482.25 °C
Endset 644.27 °C
Inflect. Pt. 523.55 °C
Inflect. Slp. -19.23e-03 %min^-1
Left Limit 373.19 °C
Right Limit 739.83 °C
Heating Rate 10.00 °Cmin^-1
Result Mode Sample Temp
n-th order Kinetics
ln(k0) 2.93 +/- 0.37
EA 65.39 +/- 2.29 kJ/mol
n 1.37 +/- 53.72e-03
Left 373.19 °C
Right 739.83 °C
Heating Rate 10.00 °Cmin^-1
Baseline Type line
Delta m -39.85 %
Result Mode Sample Temp
°C
70 min
METTLER TOLEDO
STAR° SW 19.00

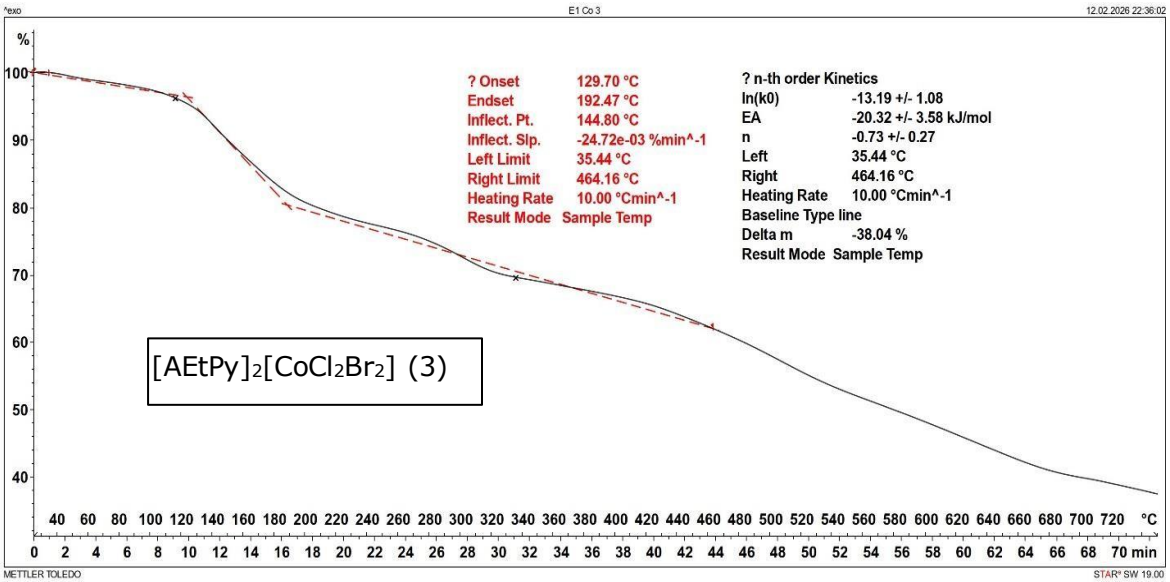
^exo
E1 Co 3
12.02.2026 22:36:02
%
? Onset 129.70 °C
Endset 192.47 °C
Inflect. Pt. 144.80 °C
Inflect. Slp. -24.72e-03 %min^-1
Left Limit 35.44 °C
Right Limit 464.16 °C
Heating Rate 10.00 °Cmin^-1
Result Mode Sample Temp
? n-th order Kinetics
ln(k0) -13.19 +/- 1.08
EA -20.32 +/- 3.58 kJ/mol
n -0.73 +/- 0.27
Left 35.44 °C
Right 464.16 °C
Heating Rate 10.00 °Cmin^-1
Baseline Type line
Delta m -38.04 %
Result Mode Sample Temp
[AEtPy]2[CoCl2Br2] (3)
°C
70 min
METTLER TOLEDO
STAR° SW 19.00

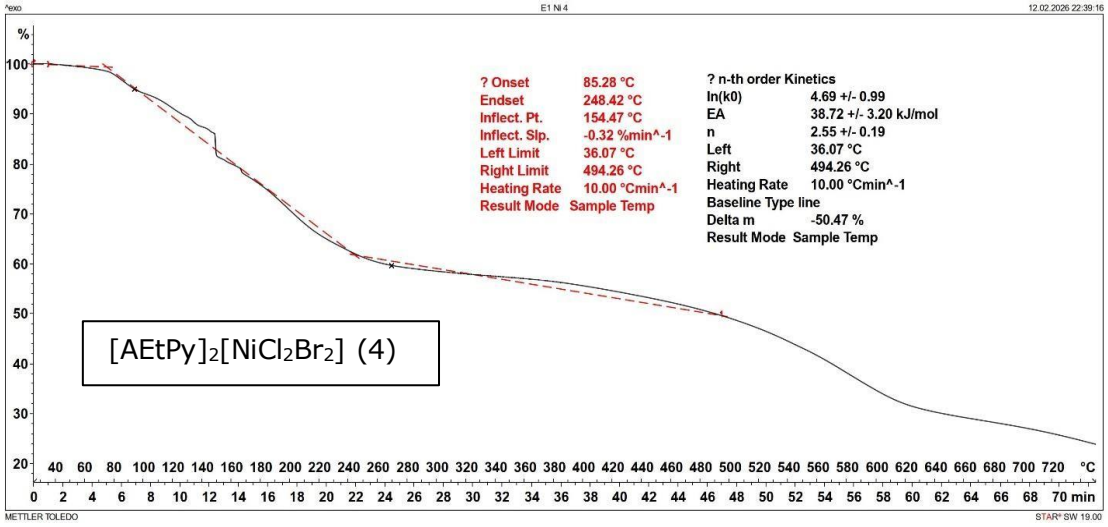
^exo
E1 Ni 4
12.02.2026 22:39:16
%
? Onset 85.28 °C
Endset 248.42 °C
Inflect. Pt. 154.47 °C
Inflect. Slp. -0.32 %min^-1
Left Limit 36.07 °C
Right Limit 494.26 °C
Heating Rate 10.00 °Cmin^-1
Result Mode Sample Temp
? n-th order Kinetics
ln(k0) 4.69 +/- 0.99
EA 38.72 +/- 3.20 kJ/mol
n 2.55 +/- 0.19
Left 36.07 °C
Right 494.26 °C
Heating Rate 10.00 °Cmin^-1
Baseline Type line
Delta m -50.47 %
Result Mode Sample Temp
[AEtPy]2[NiCl2Br2] (4)
°C
min
METTLER TOLEDO
STAR° SW 19.00

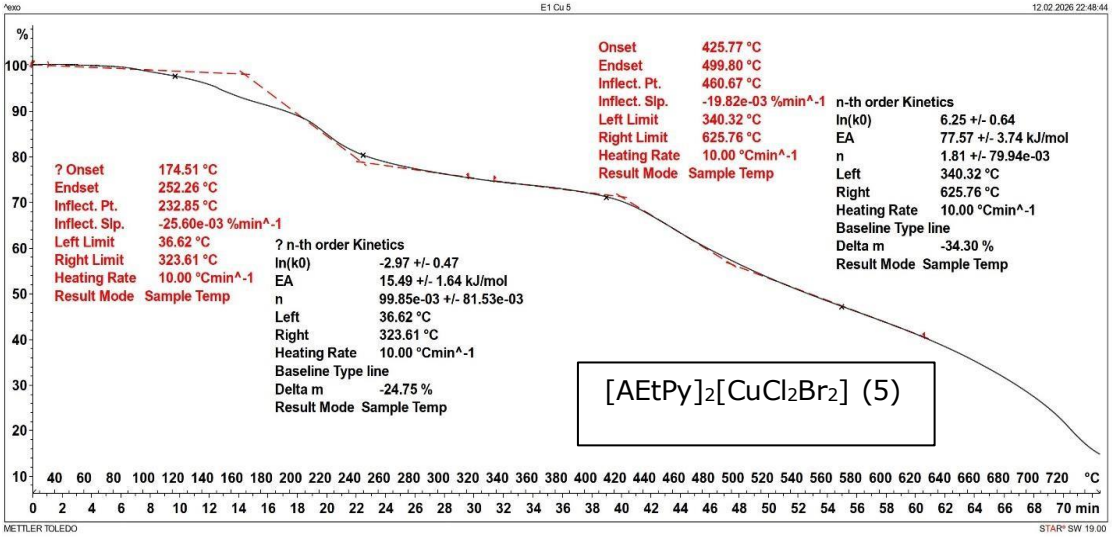
^exo
E1 Cu 5
12.02.2026 22:48:44
%
Onset 425.77 °C
Endset 499.80 °C
Inflect. Pt. 460.67 °C
Inflect. Slp. -19.82e-03 %min^-1
Left Limit 340.32 °C
Right Limit 625.76 °C
Heating Rate 10.00 °Cmin^-1
Result Mode Sample Temp
n-th order Kinetics
ln(k0) 6.25 +/- 0.64
EA 77.57 +/- 3.74 kJ/mol
n 1.81 +/- 79.94e-03
Left 340.32 °C
Right 625.76 °C
Heating Rate 10.00 °Cmin^-1
Baseline Type line
Delta m -34.30 %
Result Mode Sample Temp
? Onset 174.51 °C
Endset 252.26 °C
Inflect. Pt. 232.85 °C
Inflect. Slp. -25.60e-03 %min^-1
Left Limit 36.62 °C
Right Limit 323.61 °C
Heating Rate 10.00 °Cmin^-1
Result Mode Sample Temp
? n-th order Kinetics
ln(k0) -2.97 +/- 0.47
EA 15.49 +/- 1.64 kJ/mol
n 99.85e-03 +/- 81.53e-03
Left 36.62 °C
Right 323.61 °C
Heating Rate 10.00 °Cmin^-1
Baseline Type line
Delta m -24.75 %
Result Mode Sample Temp
[AEtPy]2[CuCl2Br2] (5)
°C
min
METTLER TOLEDO
STAR° SW 19.00

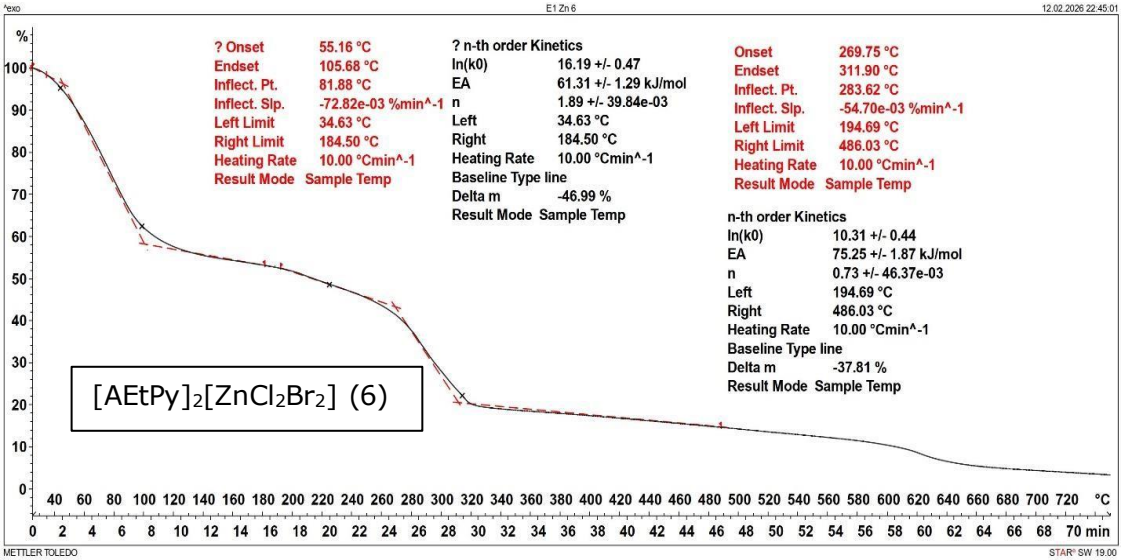
^exo
E1 Zn 6
12.02.2026 22:45:01
%
? Onset 55.16 °C
Endset 105.68 °C
Inflect. Pt. 81.88 °C
Inflect. Slp. -72.82e-03 %min^-1
Left Limit 34.63 °C
Right Limit 184.50 °C
Heating Rate 10.00 °Cmin^-1
Result Mode Sample Temp
? n-th order Kinetics
ln(k0) 16.19 +/- 0.47
EA 61.31 +/- 1.29 kJ/mol
n 1.89 +/- 39.84e-03
Left 34.63 °C
Right 184.50 °C
Heating Rate 10.00 °Cmin^-1
Baseline Type line
Delta m -46.99 %
Result Mode Sample Temp
Onset 269.75 °C
Endset 311.90 °C
Inflect. Pt. 283.62 °C
Inflect. Slp. -54.70e-03 %min^-1
Left Limit 194.69 °C
Right Limit 486.03 °C
Heating Rate 10.00 °Cmin^-1
Result Mode Sample Temp
n-th order Kinetics
ln(k0) 10.31 +/- 0.44
EA 75.25 +/- 1.87 kJ/mol
n 0.73 +/- 46.37e-03
Left 194.69 °C
Right 486.03 °C
Heating Rate 10.00 °Cmin^-1
Baseline Type line
Delta m -37.81 %
Result Mode Sample Temp
[AEtPy]2[ZnCl2Br2] (6)
°C
min
METTLER TOLEDO
STAR° SW 19.00

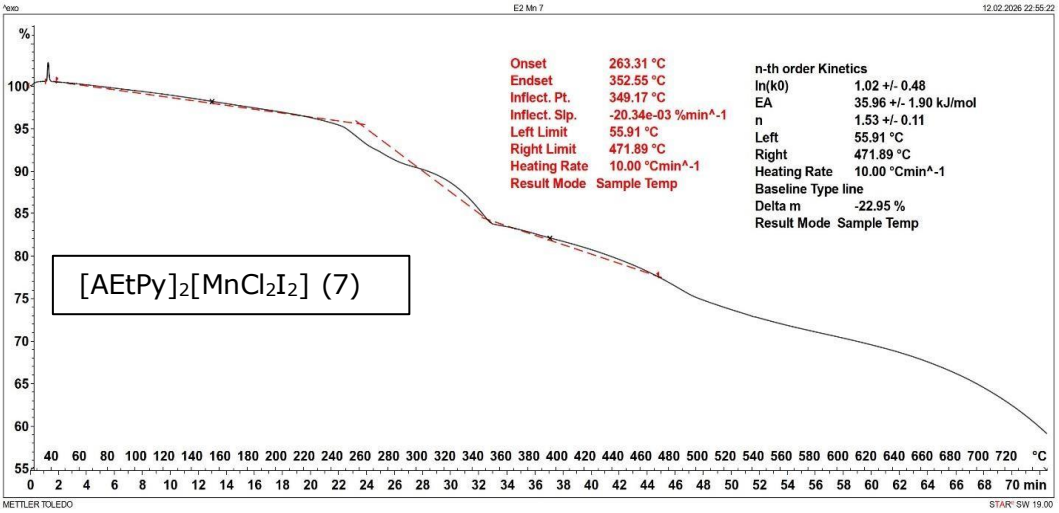
^exo
E2 Mn 7
12.02.2026 22:55:22
%
Onset 263.31 °C
Endset 352.55 °C
Inflect. Pt. 349.17 °C
Inflect. Slp. -20.34e-03 %min^-1
Left Limit 55.91 °C
Right Limit 471.89 °C
Heating Rate 10.00 °Cmin^-1
Result Mode Sample Temp
n-th order Kinetics
ln(k0) 1.02 +/- 0.48
EA 35.96 +/- 1.90 kJ/mol
n 1.53 +/- 0.11
Left 55.91 °C
Right 471.89 °C
Heating Rate 10.00 °Cmin^-1
Baseline Type line
Delta m -22.95 %
Result Mode Sample Temp
[AEtPy]2[MnCl2I2] (7)
°C
70 min
METTLER TOLEDO
STAR° SW 19.00

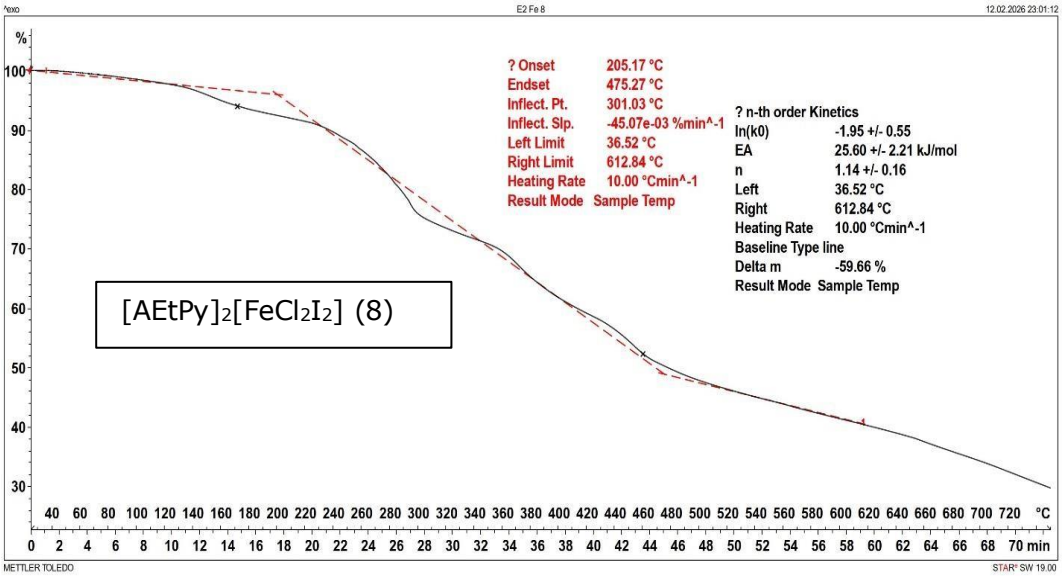
^exo
E2 Fe 8
12.02.2026 23:01:12
%
? Onset 205.17 °C
Endset 475.27 °C
Inflect. Pt. 301.03 °C
Inflect. Slp. -45.07e-03 %min^-1
Left Limit 36.52 °C
Right Limit 612.84 °C
Heating Rate 10.00 °Cmin^-1
Result Mode Sample Temp
? n-th order Kinetics
ln(k0) -1.95 +/- 0.55
EA 25.60 +/- 2.21 kJ/mol
n 1.14 +/- 0.16
Left 36.52 °C
Right 612.84 °C
Heating Rate 10.00 °Cmin^-1
Baseline Type line
Delta m -59.66 %
Result Mode Sample Temp
[AEtPy]2[FeCl2I2] (8)
°C
70 min
METTLER TOLEDO
STAR° SW 19.00

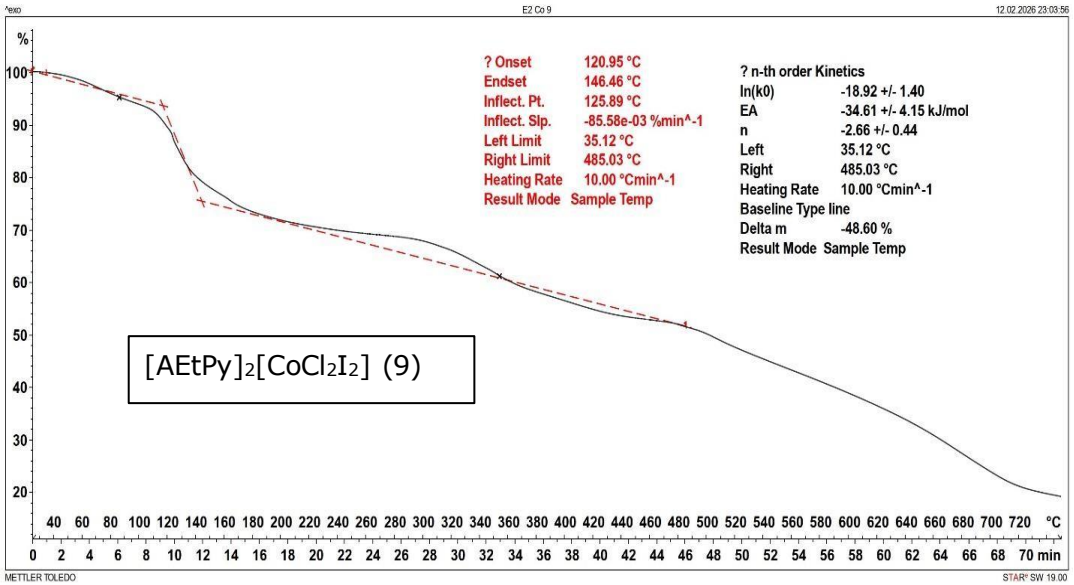
^exo
E2 Co 9
12.02.2026 23:03:56
%
? Onset 120.95 °C
Endset 146.46 °C
Inflect. Pt. 125.89 °C
Inflect. Slp. -85.58e-03 %min^-1
Left Limit 35.12 °C
Right Limit 485.03 °C
Heating Rate 10.00 °Cmin^-1
Result Mode Sample Temp
? n-th order Kinetics
ln(k0) -18.92 +/- 1.40
EA -34.61 +/- 4.15 kJ/mol
n -2.66 +/- 0.44
Left 35.12 °C
Right 485.03 °C
Heating Rate 10.00 °Cmin^-1
Baseline Type line
Delta m -48.60 %
Result Mode Sample Temp
[AEtPy]2[CoCl2I2] (9)
°C
70 min
METTLER TOLEDO
STAR° SW 19.00

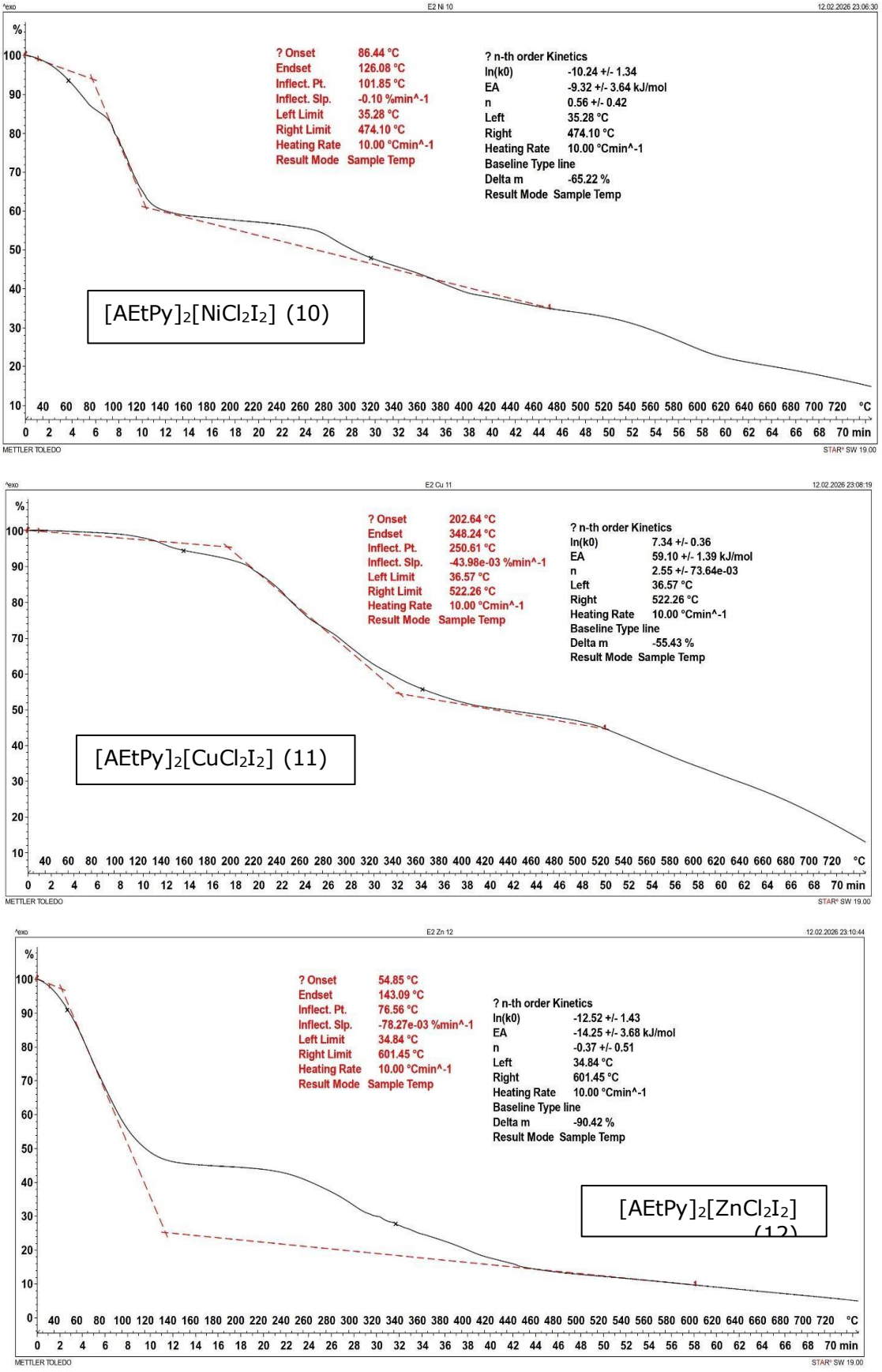

Fig. S5. The TGA curves of prepared complex salts **1-12**

References

1. Zhou T., Gui C., Sun L., Hu Y., Lyu H., Wang Z., Song Z., Yu G. Energy applications of ionic liquids: recent developments and future prospects. *Chemical Reviews*, 2023, **Vol. 123(21)**, p. 12170-12253. DOI: abs/10.1021/acs.chemrev.3c00391.
2. Greer A.J., Jacquemin J., Hardacre C. Industrial applications of ionic liquids. *Molecules*, 2020, **Vol. 25(21)**, 5207. DOI: 10.3390/molecules25215207 .
3. Hayes R., Warr G.G., Atkin R. Structure and nanostructure in ionic liquids. *Chemical Reviews*, 2015, **Vol. 115(13)**, p. 6357-6426. DOI: 10.1021/cr500411q.
4. Figueiredo N.M., Voroshylova I.V., Ferreira E.S., Marques J.M., Cordeiro M.N.D. Magnetic ionic liquids: current achievements and future perspectives with a focus on computational approaches. *Chemical Reviews*, 2024, **Vol. 124(6)**, p. 3392-3415. DOI: 10.1021/acs.chemrev.3c00678.
5. Tikhomirov A.D., Egorova K.S., Ananikov V.P. Designing Effective Antimicrobial Agents: Structural Insights into the Antibiofilm Activity of Ionic Liquids. *Journal of Medicinal Chemistry*, 2025, **Vol. 68(3)**, p. 2105-2123. DOI: 10.1021/acs.jmedchem.4c01780.
6. Ding C., Sun Z., Zhang L. Efficient removal of basic heterocyclic nitrogen compounds from fuel oils by functionalized acidic ionic liquids: Extraction experiment and interaction exploration. *Journal of Molecular Liquids*, 2023, **Vol. 386**, 122455. DOI: 10.1016/j.molliq.2023.122455.
7. Xu D., Sadrmousavi-Dizaj A., Gao J., Zhang L., Ma Y., Wang Y. Efficient extraction and theoretical insights into the separation of pyridine from simulated oil using functionalized imidazolium-based ionic liquids. *Fuel*, 2025, **Vol. 396**, 135295. DOI: 10.1016/j.fuel.2025.135295.
8. Tamilarasan R., Ganesan K., Subramani A., Benazir Ali L., Alam M.M., Mohammed A., Synthesis, characterization, pharmacogenomics, and molecular simulation of pyridinium type of ionic liquids and their applications. *ACS Omega*, 2023, **Vol. 8(4)**, p. 4146-4155. DOI: 10.1021/acsomega.2c07129.
9. Farhadi M., Sayyahi S., Gorjizadeh M. Pyridinium-Based Paramagnetic Room-Temperature Ionic Liquid for Effective Removal of Trace Olefins from Aromatics. *Advanced Journal of Chemistry, Section A*, 2021, **Vol. 4**, 188. DOI: 10.22034/AJCA.2021.272951.1241.
10. Balischewski C., Bhattacharyya B., Bailey J.J., Place S.D., Nockemann P., Kim J., Wedel A., Gahlaut S., Bald I., Li W. Elucidating the Iron-Based Ionic Liquid [C4py][FeCl4]: Structural Insights and Potential for Nonaqueous Redox Flow Batteries. *Advanced Functional Materials*, 2024, **Vol. 34(12)**, 2311571. DOI: 10.1002/adfm.202311571.
11. Chaban V.V. Acetone as a polar co-solvent for pyridinium-based ionic liquids. *RSC Advances*, 2016, **Vol. 6(11)**, p. 8906-8912. DOI: 10.1039/C5RA19511J.
12. Cipta O., Alni A., Hertadi R. Synthesis of pyridinium-based ionic liquids and their application to improve Candida rugosa lipase stability in a methanol-water solvent system. *Turkish Journal of Chemistry*, 2023, **Vol. 47(2)**, p. 307-320. DOI: 10.55730/1300-0527.3539.
13. Clarke C.J., Bui-Le L., Hallett J.P., Licence P. Thermally-stable imidazolium dicationic ionic liquids with pyridine functional groups. *ACS Sustainable Chemistry & Engineering*, 2020, **Vol. 8(23)**, p. 8762-8772. DOI: 10.1021/acssuschemeng.0c02473.
14. Ahmed M., Rao S.S., Filippov A., Johansson P., Shah F.U. Aromatic heterocyclic anion based ionic liquids and electrolytes. *Physical Chemistry Chemical Physics*, 2023, **Vol. 25(4)**, p. 3502-3512. DOI: 10.1039/D2CP05272E.
15. Foong C.Y., Wirzal M.D.H., Bustam M.A. A review on nanofibers membrane with amino-based ionic liquid for heavy metal removal. *Journal of Molecular Liquids*, 2020, **Vol. 297,** 111793. DOI: 10.1016/j.molliq.2019.111793.
16. Paucar N.E., Kiggins P., Blad B., De Jesus K., Afrin F., Pashikanti S., Sharma K. Ionic liquids for the removal of sulfur and nitrogen compounds in fuels: a review. *Environmental Chemistry Letters*, 2021, **Vol. 19(2)**, p. 1205-1228. DOI: 10.1007/s10311-020-01135-1.

17. Sabah A.A., Sulyman S.A., Aldabagh A.A., Ayoob A.K., Alsultan M., Hameed R.T. Using of benzotriazolium iodide ionic liquids for extractive desulfurization of model diesel oil. *Journal of the Turkish Chemical Society Section A: Chemistry*, 2024, **Vol. 11(4)**, p. 1641-1650. DOI: 10.18596/jotcsa.1404722.
18. Sabah A.A. Extractive desulfurization using piperidinium based ionic liquids with Lewis acids. *Journal of the Turkish Chemical Society Section A: Chemistry*, 2021, **Vol. 8(4)**, p. 1057-1088. DOI: 10.18596/jotcsa.932412.
19. Saeed I.A., Al-Asalli S.M., Saeed F.T. Synthesis and characterization of new complex salts of some transition metals with carbazolium and phosphonium salts. *Chemical Problems*, 2025, **Vol. 23(3)**, p. 563-572. DOI: 10.32737/2221-8688-2025-4-563-572
20. Wang Y., Qin C., Witarsa F. Clarifying configurations of reaction rate constant for first-order and Monod-type kinetics: a comparative manner and a pursuit of parametric definition. *Waste Management*, 2018, **Vol. 77,** p. 22-29. DOI: 10.1016/j.wasman.2018.04.040.
21. DaCosta H., Maohong F. *Rate constant calculation for thermal reactions.* 2011. Wiley Online Library. DOI: 10.1002/9781118166123.
22. Ramirez Arias A.M., Moreno-Piraján J.C., Giraldo L. Kinetic study of waste tire pyrolysis using thermogravimetric analysis. *ACS Omega*, 2022, **Vol. 7(19)**, p. 16298-16305. DOI: 10.1021/acsomega.1c06345.
23. Bafna S. On the use of Ozawa/Flynn/Wall method to determine aging activation energy for elastomers. *Journal of Elastomers & Plastics*, 2022, **Vol. 54(1)**, p. 56-66. DOI: 10.1177/00952443211020330.
24. Pereiro A., Rodriguez A., Blesic M., Shimizu K., Canongia Lopes J., Rebelo L. Mixtures of pyridine and nicotine with pyridinium-based ionic liquids. *Journal of Chemical & Engineering Data*, 2011, **Vol. 56(12)**, p. 4356-4363. DOI: 10.1021/je2001446.
25. Sabah A.A. Synthesis and characterization of some transition metals complex salts of pyridinium iodide ionic liquids: Application on extractive desulfurization. *Journal of the Turkish Chemical Society Section A: Chemistry*, 2021, **Vol. 8(3)**, p. 763-774. DOI: 10.18596/jotcsa.942318.
26. Mohammed A.F., Alyass J.M. First Transition Metal Complexes Salts of Diazonium Derived from Nitrogen Heterocyclic Compound, Synthesis, Characterization and Biological Activity. *Baghdad Science Journal*, 2024, **Vol. 21(3)**, 3. DOI: 10.21123/bsj.2023.7872.
27. Alfares A.A., Alnuaimy L.A., Al-Daher A.G.M. Synthesis and Characterization of Mn (II), Co (II), Ni (II), Cu (II) and Zn (II) complexes with 2-Carboxy benzaldehyde Aroylhydrazones. *Egyptian Journal of Chemistry*, 2022, **Vol. 65(1)**, p. 271-278. DOI: 10.21608/EJCHEM.2021.85295.4146.
28. Sabah A.A. Extractive desulfurization of model oil using 1-methyl-4-ethyl pyridinium iodide ionic liquids with some Lewis acids. *Egyptian Journal of Chemistry*, 2022, **Vol. 65(5)**, p. 147-152. DOI: 10.21608/EJCHEM.2021.94647.4450.
29. Verdía P., González E.J., Rodríguez-Cabo B., Tojo E. Synthesis and characterization of new polysubstituted pyridinium-based ionic liquids: application as solvents on desulfurization of fuel oils. *Green Chemistry*, 2011, **Vol. 13(10)**, p. 2768-2776. DOI: 10.1039/C1GC15408G.
30. Harjani J.R., Singer R.D., Garcia M.T., Scammells P.J. Biodegradable pyridinium ionic liquids: design, synthesis and evaluation. *Green Chemistry*, 2009, **Vol. 11(1)**, p. 83-90. DOI: 10.1039/B814615D.
31. Valanciene E., Miknius L., Pedisius N. The influence of zeolite catalyst on kinetics and thermodynamics of polypropylene waste thermal degradation. *Journal of Thermal Analysis and Calorimetry*, 2016, **Vol. 124(1)**, p. 341-354. DOI: 10.1007/s10973-015-5150-7.
32. Sasca V.Z., Verdeș O., Popa A. The estimation of thermal endurance for some heteropoly acidic catalysts from thermogravimetric decomposition data. *Journal of Thermal Analysis and Calorimetry*, 2017, **Vol. 127(1)**, p. 273-282. DOI: 10.1007/s10973-016-5479-6.